Palaeogeography, Palaeoclimatology, Palaeoecology 602 (2022) 111163

Contents lists available at ScienceDirect

Palaeogeography, Palaeoclimatology, Palaeoecology

journal homepage: www.elsevier.com/locate/palaeo

# Foraminifera indicate Neogene evolution of Yongle Atoll from Xisha Islands in the South China Sea

Min Meng [a], Kefu Yu [a,*], Pamela Hallock [b], Guoquan Qin [c], Wei Jiang [a], Tianlai Fan [a]

[a] Guangxi Laboratory on the Study of Coral Reefs in the South China Sea, Coral Reef Research Center of China, School of Marine Sciences, Guangxi University, Nanning, Guangxi 530004, China
[b] College of Marine Science, University of South Florida, St. Petersburg, FL 33701-5016, USA
[c] East China Sea Research Institute of CNOOC Research Center, China

ARTICLE INFO

Editor : S. Shen

*Keywords:*
Coral reefs
Biostratigraphy
Carbonate facies
Paleoecology
Paleobathymetry

ABSTRACT

The study presents a detailed record of foraminiferal faunas from CK2 core, a 928.75 m long core drilled in the center of Xisha Islands, South China Sea, for biostratigraphy and palaeoenvironmental reconstruction of the study area. Coupling foraminiferal biostratigraphy and bulk-sediment strontium-isotope chronologic age revealed that carbonate deposition occurred from Early Miocene (~19.6 Ma) to present. Examination of 281 petrologic thin sections and 246 unconsolidated sediment samples revealed 141 foraminiferal taxa, among which the foraminiferal abundance and simple diversity peaked in the Middle Miocene and Pliocene to early Pleistocene strata. Nine foraminiferal assemblages (FAs) were distinguished, documenting eight distinct facies that indicated five intervals in the development of Xisha Islands. At the initial interval (19.6–17 Ma), a coral, coralline algal and shallow-water larger foraminifers (FA1 and FA2) association colonized the shallow platform facies, forming an aggrading sequence in response to tectonic subsidence and sea-level rise. Platform development slowed from 17 to 10.19 Ma, dominated by the miliolids and small benthic foraminifers as well as larger benthic foraminifers (FA3 and FA4) representing lagoonal to reef-flat facies with agradation to progradation (backreef infilling) associated with sea-level fall. At 10.19–4.35 Ma, a deepening sequence was indicated by the change from shallow-water benthic foraminifers (FA5) upward to deeper dwelling species (FA6), as a result of climatic cooling and abrupt sea-level fluctuation. As sea level rose, the platform was drowned from 4.35 to 2.18 Ma, as indicated by abundant planktic foraminifers and large, flat benthic foraminifers (FA7 and FA8). At 2.18–0.089 Ma, the platform aggraded rapidly with sea level fall indicated by the appearance of thick benthic foraminifers (FA9) and increased coral. The close association between the biofacies and regional paleobathymetry, which was in phase with the long-term global sea-level change, suggest that foraminiferal morphology and assemblage composition are ideal parameters for paleobathymetric and paleo-depositional environmental interpretations.

## 1. Introduction

Reef-associated foraminifers, the super-abundant and diverse microorganisms in tropical shallow-water carbonates, are powerful tools for stratigraphic and paleo-environmental studies. Planktic foraminifers and larger benthic foraminifers are extensively used as biostratigraphic markers in pelagic and neritic environments due to their rapid diversification and abrupt species turnover (e.g. Blow, 1979; Bolli and Saunders, 1985; Berggren et al., 1995; Boudagher-Fadel and Banner, 1999; Renema, 2007; BouDagher-Fadel, 2008; Boudagher-Fadel, 2018; Wade et al., 2011; Gradstein et al., 2012). Due to their sensitivity to physiochemical environmental condition, including light, temperature, salinity, substrate, pH, and food resources, the reef-associated benthic foraminifers, with distinct depth ranges preferences, changed spatially and temporally through the history of carbonate deposition (Hohenegger, 2004, 2005; Murray, 2006; Renema, 2017). Therefore, foraminiferal faunal analysis, including abundance, diversity, assemblages, and morphologies, are outstanding proxies for prevailing palaeoenvironmental conditions of carbonate-platform successions, especially bathymetric variation (e.g. Hallock and Glenn, 1985; Beavington-Penney and Racey, 2004; Renema, 2017). For example, larger benthic foraminifera, which mostly host algal endosymbionts, are excellent indicators of depth within the photic zone in tropical to warm temperate, shelf and upper slope waters. The depth dependence is mirrored in a

* Corresponding author.
*E-mail address:* kefuyu@scsio.ac.cn (K. Yu).

https://doi.org/10.1016/j.palaeo.2022.111163
Received 30 January 2022; Received in revised form 21 July 2022; Accepted 24 July 2022
Available online 29 July 2022

combination of their morphology traits (e.g., size, degree of flatness and wall structure) influenced by hydrodynamic forces and light intensity (Hallock and Glenn, 1986; Hohenegger and Yordanova, 2001). In contrast, some small benthic foraminifers tolerate unstable physico-chemical conditions and thrive in more quiet environments. They tend to be more prevalent in backreef-lagoon or leeward reef-slope facies (Abu-Zied and Bantan, 2013; Anbuselvan, 2019). Planktic foraminifers are indicators of open marine environment with slope and basin facies (Geel, 2000). In all, reef-associated foraminifers provide an invaluable "endoscope" for observing and interpreting the environmental, ecological, and bathymetric conditions in modern and ancient carbonate platforms.

Several studies have conducted foraminiferal biostratigraphic and palaeoenvironment research in deep drillings of Xisha Islands (Fig. 1), including XY1 (Qin, 1987), XY2 (Meng, 1989), XC1 (Meng, 1989; Han and Meng, 1990; Wang et al., 1996), XK1 (Ma et al., 2017) and XS1 (Qin and Zhu, 1982). However, lacking chronological control of planktic or larger benthic foraminiferal biostratigraphy and without considering the analogy with modern reef foraminiferal biozonation as well as other biological components, detailed interpretation of the evolution of sedimentary facies of Xisha Islands was not possible. In addition, uncertainties remain about the amplitude of paleo-water depth change.

The Chenke-2 (CK2) core was drilled on the reef flat of Chenhang Island, Yongle Atoll, west of Xisha carbonate platform (Fig. 1), penetrating the 873.55 m-thick carbonate succession unconformably overlying the 52.2 m-thick volcano-clastic rock. The thick accumulation of sediments with high recovery (average 70%) and relatively consecutive stratigraphy yielded ideal materials to elucidate the development of the Xisha carbonate platform (Fan et al., 2020). Our objectives were to: (1) develop a well-constrained stratigraphic model of CK2 by synthesizing planktic and larger benthic foraminiferal biostratigraphy with Sr-isotope chronology; (2) interpret the carbonate succession with the combination of stratigraphic, sedimentological and biological analysis; (3) reconstruct paleobathymetry by describing temporal changes in foraminiferal assemblages and sediment facies, along with grain-size proxies, and (4) determine paleoenvironmental correlates (such as tectonic activity, eustasy, nutrient flux and paleoclimatic change) with the long-term changes in carbonate production.

## 2. Regional geological and geographical settings

The Xisha Islands (15°46′–17°08′N, 111°11′–112°54′E) occur on a coral-reef dominated carbonate platform, located on the west and southwest of the Xisha uplift, in the northwestern South China Sea (SCS) (Fan et al., 2020). The Xisha uplift formed during the late Cretaceous to early Oligocene associated with seafloor spreading in the SCS. The deep, hemiplegic troughs (>1000 m), which developed between the Xisha uplift and the South China block, isolated Xisha from terrestrial influence, resulting in an autochthonic reef system well-suited for documenting natural evolution.

During the late Oligocene to early Miocene, post-rift thermal subsidence generated a neritic environment on the Xisha uplift that suitable for warm-water, carbonate-producing organisms. Platforms extensively developed and aggraded in the Middle Miocene in response to subsidence and sea-level rise, then mostly drowned in the Late Miocene except the central Xisha uplift, where larger atolls developed, including Yongle atolls and Xuande atolls (Wu et al., 2014, 2016). This drowning is in contrast with documented Late Tortonian to Messinian eustatic lowstands in other regions (Zachos et al., 2001; Haq et al., 1987); Wu et al. (2016) linked the late Miocene carbonate drowning to higher rates of subsidence.

Xisha Islands is situated in the tropical convergence band, with annual mean sea surface temperature 26.8 °C and the annual mean sea surface salinity 33.7 p.s.u., which has been beneficial to the

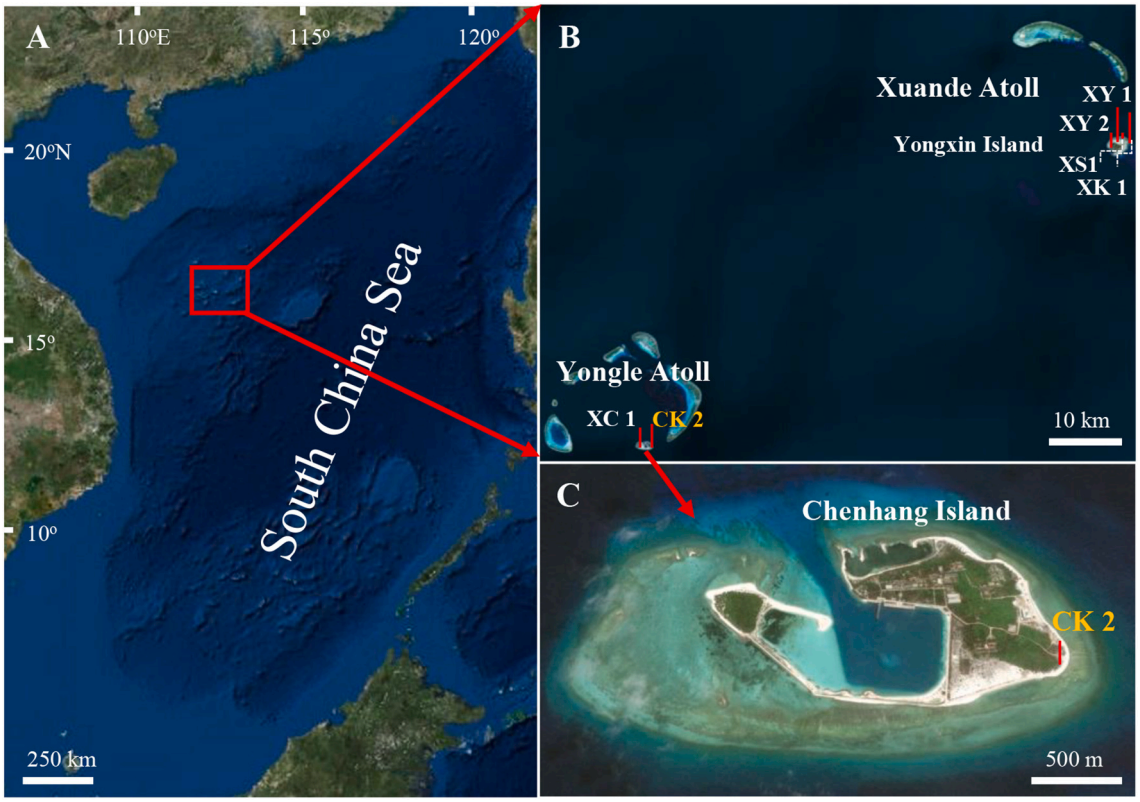


**Fig. 1.** Locality map of CK2 core on the Chenhang Island and the previous drill holes (XY1-Xiyong 1, XY2-Xiyong 2, XK1-Xike 1, XS1-Xishi 1, XC1-Xichen 1). A: Location of Xisha Islands in the SCS. B: Distribution of Yongle Atoll and Xuande Atoll on Xisha Islands, and the cores mentioned in this study. C: Location of CK2 on Chenhang Island. The depth of the cores were scaled down.

development of carbonate factories. The location is also in the East Asia monsoon region, southwestern-southeastern monsoon dominates from May through September, and northeast monsoon from October to the following March. During the monsoon seasons, storms produce ocean swells, resulting in highly hydrodynamic conditions on the windward sides of the platforms. The surficial sediments of modern coral reef in Xisha Islands are mainly composed of corals, coralline algae, and benthic foraminifera, associated with mollusks, bryozoans, echinoids, and sponges.

## 3. Methods and materials

Thin sections (281, 48 × 28 mm in size) were prepared at 3 m intervals along the core for microfacies analysis and identification of foraminifers. Microfacies analysis included lithological classification and semi-quantitative determination of the abundance of most skeletal components, that is, measuring the proportional area occupied by each biogenic population relative to the whole slide surface. The classification of carbonate rocks followed the textural schemes of Dunham (1962) and Embry and Klovan (1971). The identification of bioclastic components followed Scholle and Ulmer-Scholle (2003), Flügel (2010), and BouDagher-Fadel (2008). When present, larger benthic foraminifers in thin sections were identified to genus or species level, based on external test morphology, with additional oriented thin sections for the identification based on internal morphology. Identification of smaller foraminifers and other organisms were performed at genus or family level.

To overcome the limitations of accurately identification of some smaller and planktic foraminifers in thin sections, as well as the difficulty to disaggregate strongly lithified bulk samples, the comprehensive analysis of thin sections and poor-unconsolidated sediments were made to confirm the result of foraminiferal identifications. Poorly lithified sediments were collected as bulk samples (246 samples, approximately 3 m interval) for analysis of foraminiferal assemblages and sediment textures. Each 15 g sample of air-dried sediment was soaked in water for about two weeks, then washed through 0.063 mm mesh sieves and oven-dried at 40 °C. The dried residual fractions were weighed to obtain the percentage of mud (silt + clay), then sieved through 0.125-, 0.25-, 0.5-, 1-, 2-mm graded sieves to determine the grain-size distributions. The grain-size parameters (mean grain size, sorting) were calculated using the formulas of Folk and Word (1957). Then the portions of 0.125-, 0.25-, 0.5-, 1-, 2-mm dry sediment were aggregated for foraminiferal analysis. Specimens in bulk samples were determined to the lowest taxonomic level possible (genus or species) under a binocular microscope using resources from Baker (1960), Cheng and Zheng (1978), Zheng (1979), Loeblich (1987), He and Hu (1995), and BouDagher-Fadel (2008). For quantitative analysis and comparison of assemblages among different sections, foraminifers were grouped at the genus or species levels according to their specific environmental characteristics.

To obtain insight into depositional environments, test thickness to diameter (T/D) ratios of appropriate larger foraminifers, planktic/benthic ratios (P/B), foraminiferal abundance and species number were calculated. For thin sections, all foraminiferal specimens present were summed as foraminiferal abundance (ind./slide), including benthic foraminiferal abundance and planktic ones; and benthic foraminiferal species were counted as much as possible. For poor-unconsolidated sediments, sediment fraction was split to obtain about 300 foraminifers tests. When the fractions have not enough foraminifers, all 15 g of sediment were counted. Then the benthic and planktonic foraminiferal abundance and species number were standardized to ind./g and species/g. Thickness to diameter ratios (T/D) of appropriate larger, algal-symbiont-bearing, benthic foraminifers were used to evaluate palaeobathymetry and paleohydraulics, as thicker tests are produced in turbulent and high-light (shallow) environments (e.g. Hallock and Glenn, 1985; Renema, 2005; Mateu-Vicens et al., 2009). The complete axial to subaxial sections of *Amphistegina* and lepidocyclinids specimens, that are most consistent in the whole core or in the Miocene phase, were chosen to measure the two dimensions in thin sections: thickness and diameter (also known as maximum and minimum diameters). The P/B values are considered as an indicator of changes in water depth or restricted environments (Murray and Lee, 1991); these ratios are expressed as a calculation of the percentage of planktic foraminifers in the total foraminiferal population (Nigam and Heriques, 1992):

$$[P/(P+B) \times 100\%]$$

where P is for the percent of planktic foraminifers and B is for benthic foraminifers.

The age model was developed using well-established biostratigraphic events along with the Sr- isotope timescale of Fan et al. (2020). For biozonation and correlation, temporal patterns in origination and extinction of index foraminifers were investigated. The planktic foraminiferal biostratigraphy was according to Blow (1979) and Berggren et al. (1995) as modified by Wade et al. (2011), Li et al., 2005, and Wang et al., 2003, using the time scale defined by Gradstein et al. (2012). The benthic foraminiferal biostratigraphy was defined by the East Indian "letter stage" (Adams, 1970; Boudagher-Fadel and Banner, 1999; Renema, 2007; Boudagher-Fadel et al., 2010; BouDagher-Fadel, 2018).

## 4. Results

### 4.1. Foraminiferal biostratigraphy of the core succession

The chronology of the CK2 integrates the published high resolution Sr-isotope ages (Fan et al., 2020) with biostratigraphic ages for planktic and larger benthic foraminifers (Fig. 2), assisted by lithological analyses. Larger benthic foraminiferal stratigraphy, based on the East Indian Letter Classification, was only diagnosed in the lower Miocene strata in CK2, because the upper Miocene strata were strongly dolomitized. Two biozones (Te5 and Tf1) based on large benthic foraminifers were recognized. The absence of *Austrotrillina striata* in the presence of *Austrotrillina howchini*, and the last occurrence (LO) of *Eulepidina* at the drilling depth of 780.55 m together indicated the top of Te5 stage, corresponding to the base of planktic foraminiferal biozone N7, with the age 17.62 Ma (Boudagher-Fadel and Lokier, 2005; Renema, 2007; Wade et al., 2011). The LO of *A. howchini* at 539 m defined the top of Tf1 stage in the Middle Miocene, corresponding to the top of N12 of planktic foraminiferal stratigraphy. This datum was assigned with the ages of 13.9 Ma (Berggren et al., 1995; Boudagher-Fadel and Lokier, 2005; BouDagher-Fadel, 2018). *Nephrolepidina* (LO), which appeared at 531 m in CK2, was not used as a diagnostic taxon, as that genus had been recorded in the Pliocene in XY1 core in the SCS and in Southeast Asia (Qin, 1981; Adams, 1984; Betzler and Chaproniere, 1993).

Planktic foraminifers were continuous and well-preserved in the Pliocene section. Their distributions enabled recognition of three biozones (N21, N20 and N19). The first occurrence (FO) of *Globorotalia truncatulinoides* at 228 m is well constrained at about 2 Ma (top of foraminiferal zone N21) (Berggren et al., 1995; Li et al., 2005). The LO of *Globoquadrina altispira* occur at 243 m, bears an age of about 2.8 Ma within Zone N21 in the north of the SCS (Qin, 1996). The *Sphaeroidinellopsis seminulina* (LO) at 264 m defined the top of foraminiferal zone N20 at ODP Site 1143, corresponding to an age of 3.14 Ma (Wang et al., 2003). The LO of *Globorotalia margaritae* at 276 m is a good marker for the top of N19, at 3.58 Ma (Berggren et al., 1995; Li et al., 2005). The LO of *Globigerina nepenthes* at 297 m, marks the age of about 4.2 Ma at ODP Site 1143 in the south of SCS (Berggren et al., 1995; Li et al., 2005). The FO of *Globorotalia tumida* at 306 m represents the lower boundary of N18 with the age about 5.51 Ma in the Pacific region (Wade et al., 2011).

Overall, the results of the planktic and larger benthic foraminiferal biostratigraphy are in agreement with the preliminary Sr-isotope age on the whole (Fig. 3). Based on the age model from the combination of biostratigraphy and Sr chronology, the average sedimentation rate of the carbonate section of the core (with age span of about 19.6 Ma) was

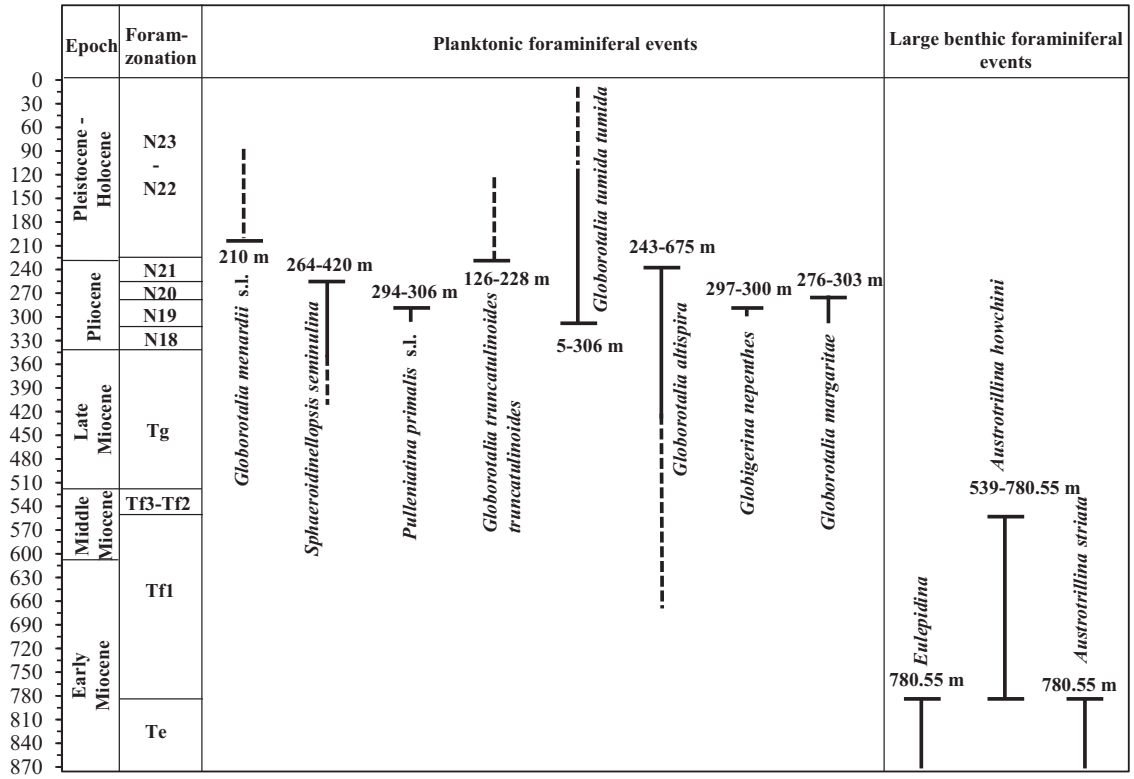


**Fig. 2.** Significant planktic foraminiferal and larger benthic foraminiferal ranges in CK2, correlated with planktic foraminiferal biozone (Blow, 1979; Bolli and Saunders, 1985; Wang et al., 2003; Li et al., 2005) and larger benthic foraminiferal biozone "Letter Stages" (BouDagher-Fadel, 2008; Renema, 2007). S.L = sinistral coiling.

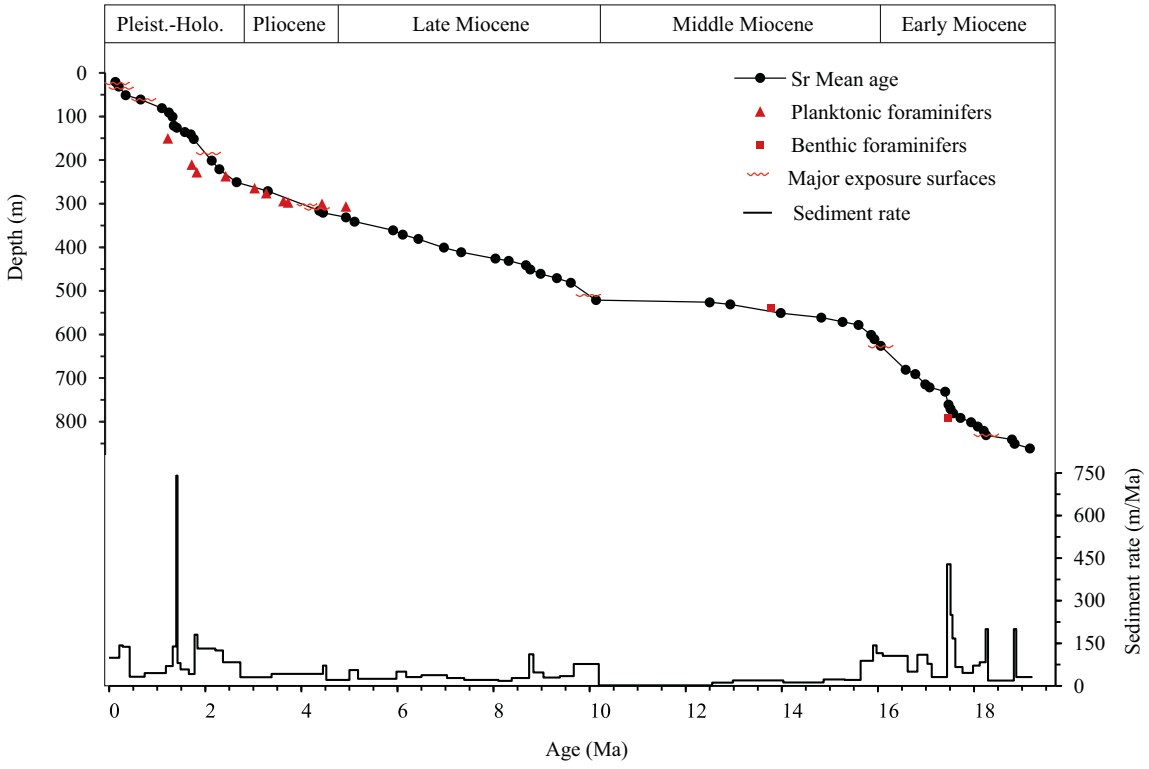


**Fig. 3.** Age-depth plot of the CK2 core (upper), incorporating Sr-isotope data (circles) (Fan et al., 2020), planktic foraminiferal biostratigraphic events (triangles), and benthic foraminiferal biostratigraphic events (squares); and age-sedimentation accumulation rate chart (lower). Depths represent drilling depth.

obtained. In the middle Early Miocene–lower Early Miocene (873.55–713 m), the average sedimentation rate was approximately 73 m/Ma. Then it decreased to roughly 41 m/Ma from the lower Early Miocene to the upper Late Miocene (713–521 m). From the upper Late Miocene–early Pliocene (521–312 m), the rate dropped further to about 28 m/Ma, and then increased somewhat to 34 m/Ma in the remainder of the Pliocene–early Pleistocene (312–198 m). Subsequently, (198–0 m), the average sedimentation rate abruptly increased to 102 m/Ma.

### 4.2. Variations in foraminiferal fauna

A total of 141 foraminiferal taxa (101 benthics and 40 planktics) were determined, representing 74 genera (61 benthics and 13 planktics). Among the identified species (6 agglutinated, 21 porcelaneous, and 74 hyaline benthics; and 40 planktics), the calcareous hyalines were predominant in most of the samples, except in the Middle Miocene–lower Late Miocene strata, where porcelaneous tests predominated. Planktic foraminifers are most frequent from the Pliocene–early Pleistocene strata (Figs. 4, 5). The benthic foraminiferal abundance (ind./g) and diversity (species/g) varied widely from 0 to 228 and 0–0.4 respectively, with two high values in the Middle Miocene and the Pliocene strata, and two low ones in the Late Miocene and Quaternary strata (Fig. 5). The P/B ratio was low (averaging 5%) with small amplitude in the Miocene strata; and peaked (averaging ~29%) from Pliocene to early Pleistocene, and subsequently decreased sharply (Fig. 6).

By frequency of occurrence, the most consistent taxa were *Amphistegina* spp. (*A. lobifera*, *A.lessonii*, *A.radiata* or *A.papillosa*), that occurred in nearly 75% of the samples recovered. Other common taxa include *Nummulites*, *Operculina complanata*, *Cycloclypeus*, *Miogypsina*, *Sorites*, *Nephrolepidina*, *Heterolepa praecinctus*, *Gypsina globula*, *Planorbulinella larvata*, *Lenticulina suborbicularis*, *Pararotalia praecalcar*, *Anomalina colligera*, *Eponides repandus*, *Borelis*, *Alveolinella*, *Globorotalia menardii*, and *Globigerinoides trilobus* (some taxa are illustrated in Figs. 7-11). Significant benthic foraminifera that mainly appeared in Miocene included *Lepidocyclina*, *Nephrolepidina*, *Eulepidina*, *Miogypsina*, *Austrotrillina*, *Flosculinalla*, *Katacycloclypeus*, *Miolepidocyclina*, and *Spiroclypeus*, others are common taxa from modern Xisha Islands (Meng et al., 2020).

### 4.3. Variations in foraminiferal assemblages

Nine major foraminiferal assemblages (FAs) were distinguished in the CK2 core (Fig. 5). The subdivision is primarily based on changes in foraminiferal abundance, diversity, the occurrence of the characteristic genera and species, and foraminiferal morphology, as described below.

#### 4.3.1. miogypsinids–lepidocyclinids assemblage (FA1: 873.55–838 m, 19.60–18.80 Ma; 768–737.12 m, 17.54–17.38 Ma)

The intervals consist of coralline rudstone and floatstone, along with coral framestone. The bioclastic components are dominated by coralline algal fragments (ranging in abundance from 0 to 65%, median 30%), and variable amounts of coral (0–100%, median 20%), with subordinate amounts of foraminifera (0–40%, median 10%), and bryozoans appear occasionally as minor components. Foraminiferal tests were medium-poorly preserved with low abundances (0–26 specimens/slide, median 7) and species number (0–9 species/slide, median 4). Most of them were hyaline species, and sporadic planktic specimen. The dominant foraminiferal taxa were *Miogypsina* (4–44%, median 21%) and lepidocyclinids (0–60%, median 25%), with few *A. lobifera* occurring. The lepidocyclinids are represented chiefly by *Nephrolepidina verbeeki*, *Nephrolepidina morgani* and *Nephrolepidina sumatrensis*. The median thickness/diameter ratio of *Amphistegina* was 0.42, and of lepidocyclinids was 0.34. Geniculate coralline algae, including *Corallina*, *Jania*, *Amphiroa,* and crustose taxa such as *Lithoporella* and *Aethesolithon,* are dominant.

#### 4.3.2. lepidocyclinids–Amphistegina–SBF (smaller benthic foraminifera) assemblage (FA2: 838–768 m, 18.8–17.52 Ma; 737.12–716 m, 17.38–17.05 Ma)

This succession included yellowish-green to greyish-green foraminiferal rudstone, wackestone, and grainstone, with more foraminifera (ranging in abundance from 0 to 60%, median 20%) and less coralline algae (0–50%, median 13%), as well as common molluscan (0–10%, median 5%) and few echinoderm (0–5%, median 2%) fragments, compared to the lower section. The foraminifers are poor-medium preserved with abundance and species number of 0–203 specimens/gram (median 53) and 0–23 species/100 g (median 14), respectively. The assemblage is characterized by abundant *Nephrolepidina*, *A. lobifera,* and smaller hyaline taxa, such as, *Anomalinella rostrate*, *Rosalina terquemi*, *Planorbulinella larvata*, *Heterolepa praecinctus* and *Cibicides*. Accessory taxa were *Miogypsina*, *Cycloclypeus*, miliolids, *Sorites* and some *Textularia*. Perforate (hyaline) foraminifers were totally dominant (median 90.9%), with slightly increased occurrences of planktic (0–14.3%) and imperforate specimens. The T/D value of *Amphistegina* varied from 0.38 to 0.66 with median value of 0.54, and lepidocyclinids 0.39–0.71 with median value 0.53. The coralline algae are mainly represented by melobesioids, such as *Mesophyllum* and *Lithothamnion,* as well as some rhodoliths.

#### 4.3.3. miliolids–small rotaliines assemblage (FA3: 703–596 m, 16.93–15.77 Ma ; 560.07–521 m , 14.79–10.19 Ma)

In this section, bioclastic rudstone and floatstone alternated with foraminiferal wackestone and packstone. Benthic Foraminifera were the most dominant components of this section (0–75%, median 31%), followed by coralline algae (0–70%, median 15%), with common coral blocks (0–90%, median 5%). The benthic foraminiferal tests, showing poor-medium preservation, increased upward with variable in

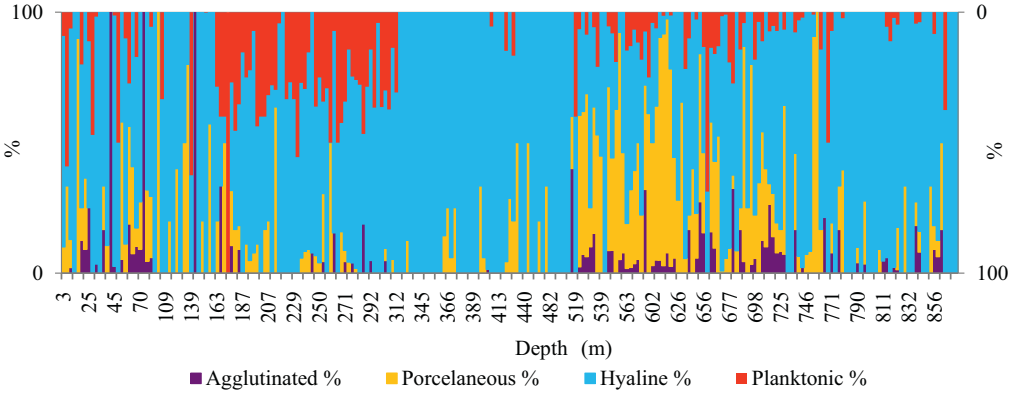


**Fig. 4.** The temporal sequence showing proportions of the benthic foraminiferal wall structural types, and the planktic foraminifers from CK2 core.

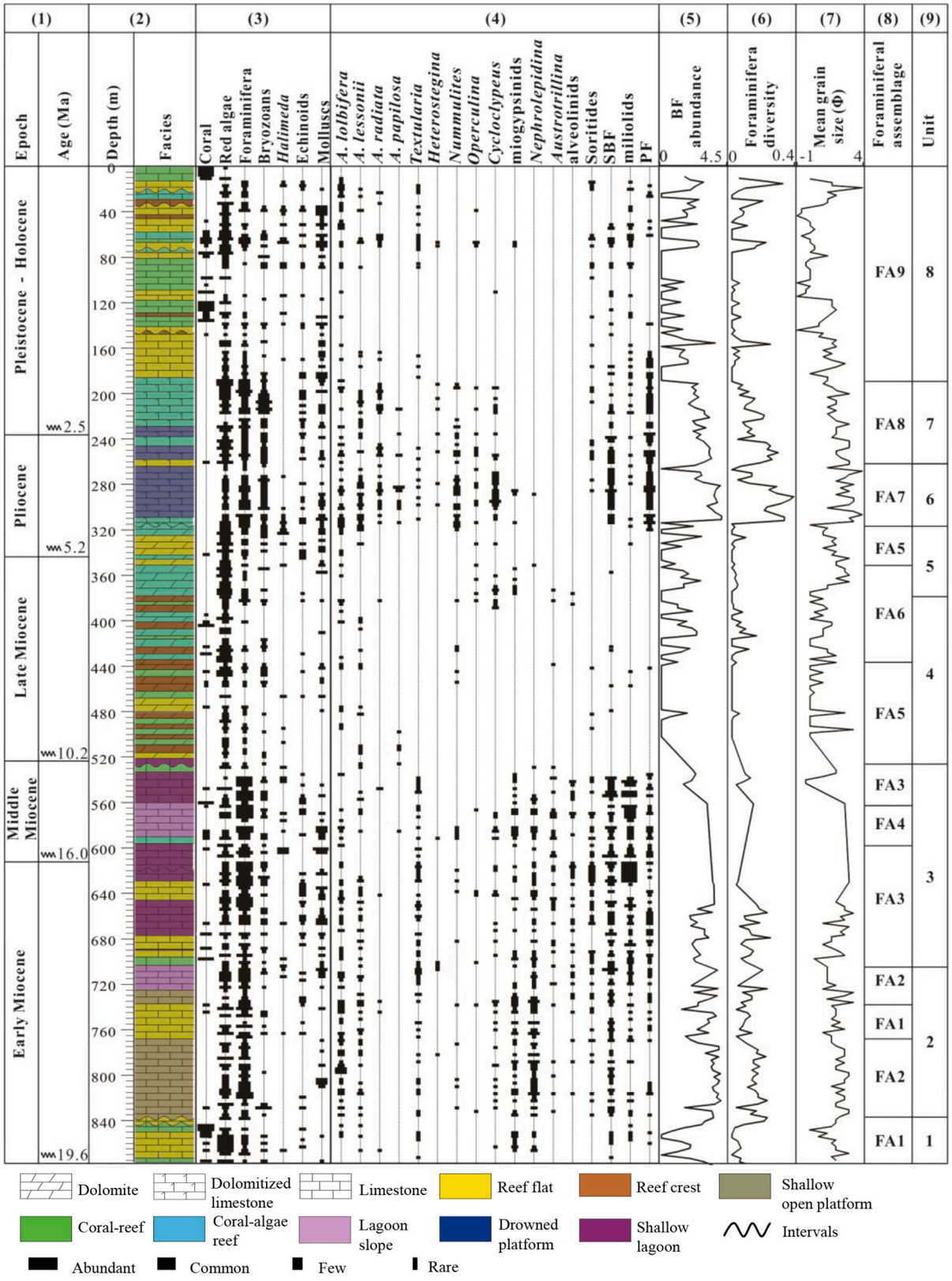


**Fig. 5.** Summary diagram indicating the sedimentary facies evolution since early Miocene using bio-constituents and foraminifera (1) Chronostratigraphy based on Sr isotopes and foraminifera; (2) facies; (3) abundance of some biological components, including coral, red algae, foraminifera, bryozoans, *Halimeda*, echinoderms, and mollusks; (4) abundance of some special foraminiferal taxa, SBF: small benthic foraminifers, PF: planktic foraminifers; (5) the log10 of benthic foraminiferal abundance (ind./100 g); (6) foraminiferalspecies number (species/g); (7) mean grain size curve; (8) foraminiferal assemblages; and (9) unit. (For interpretation of the references to colour in this figure legend, the reader is referred to the web version of this article.)

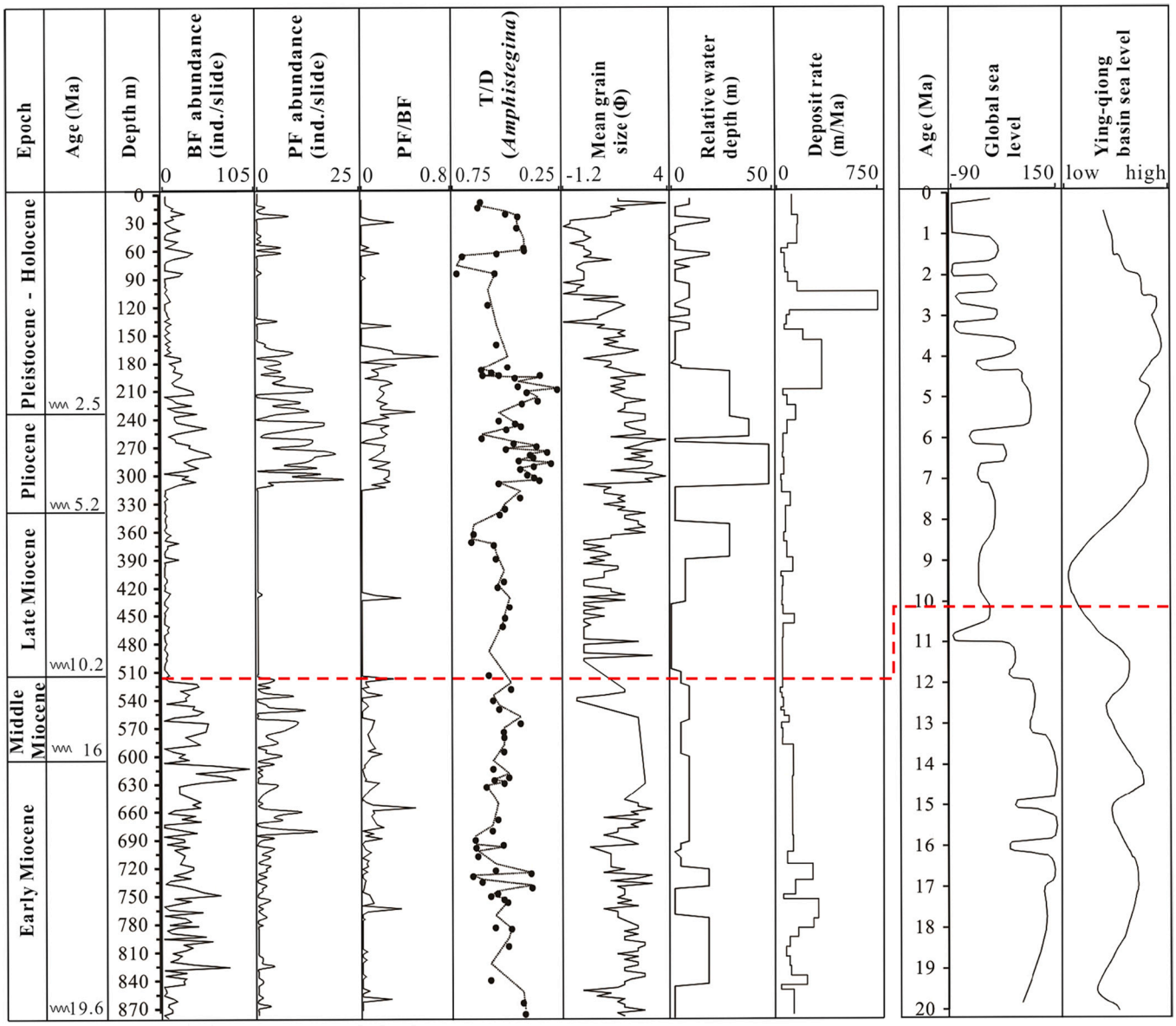


**Fig. 6.** Summary diagram indicating the change of relative water depth since early Miocene and its comparison with global sea-level curve (Haq et al., 1987) and the relative sea-level curve (Hao et al., 2000) in drill hole in the SCS, using stratigraphic distribution of the following: benthic foraminiferal abundance (ind./slide), the abundance of planktic foraminifers (ind./slide), the ratio between the numbers of planktic foraminifers and benthic foraminifers, thickness/diameter of *Amphistegina*, mean grain size curve, relative water depth and carbonate deposition ratio.

occurrence (3–113 specimens/g) and species number (3–25 species/100 g). Planktic foraminifers were scarce. From the lower section (710–677 m) to the upper part (677–521 m) miliolids and smaller benthics significantly increased replacing lepidocyclinids and *Amphistegina*. Miliolids had their highest abundance in this interval, mostly including *Quinqueloculina* spp. (*Quin.seminula*, *Quin.lamarckiana,* and others), *Triloculina* spp. (*Tr. trigonula*, *Tr. tricarinata* and others) and *Pyrgo* cf. *striolata*. The smaller hyaline foraminifers were mostly *Heterolepa*, *Robulus*, *Lenticulina suborbicularis*, *Ammonia beccarii* and *Cibicides*. The T/D of *Amphistegina* was 0.52–0.71, with a median value of 0.57, and the T/D of lepidocyclinids ranged from 0.23 to 0.56, with median value of 0.39. The shallow back-reef species, *Jania* and some *Lithoporella*, were the dominant coralline algae.

*4.3.4. lepidocyclinids–Miogypsina–miliolids assemblage (FA4: 716–703 m, 17.05–16.93 Ma; 596–560.07 m, 15.77–14.79 Ma)*

The succession consists of medium to coarsely consolidated bioclastic rudstone. Benthic foraminiferal abundance and species numbers ranged from 0 to 64 speciesmen/slide and 0–20 species/slide respectively. Planktic foraminifers were scarce. The foraminiferal assemblage was dominated by larger benthic foraminifers, such as *Nephrolepidina* and *Miogypsina.* Small benthic foraminifers that imply back reef sheltered conditions or sea grass flats environment were developed, such as miliolids and small rotaliines, including *Quinqueloculina*, *Triloculina*, *Austrotrillina*, *Planorbulinella*, *Sorites* and others. Benthic foraminifera and coralline algal were predominant compoents, with common Acropora coral branches and mollusk.

*4.3.5. Amphistegina assemblage (FA5: 521–434 m, 10.19–8.49 Ma; 344–312 m, 5.30–4.28 Ma; 264–258 m,3.15–2.99 Ma)*

The succession starts with tan, well-indurated, medium to coarsely consolidated crystalline dolomitized mudstone (521–434 m), topped by primrose-gray dolomitized packstone and wackestone (348–312 m). In the lower section (521–434 m), when heavily dolomitized, all aragonitic

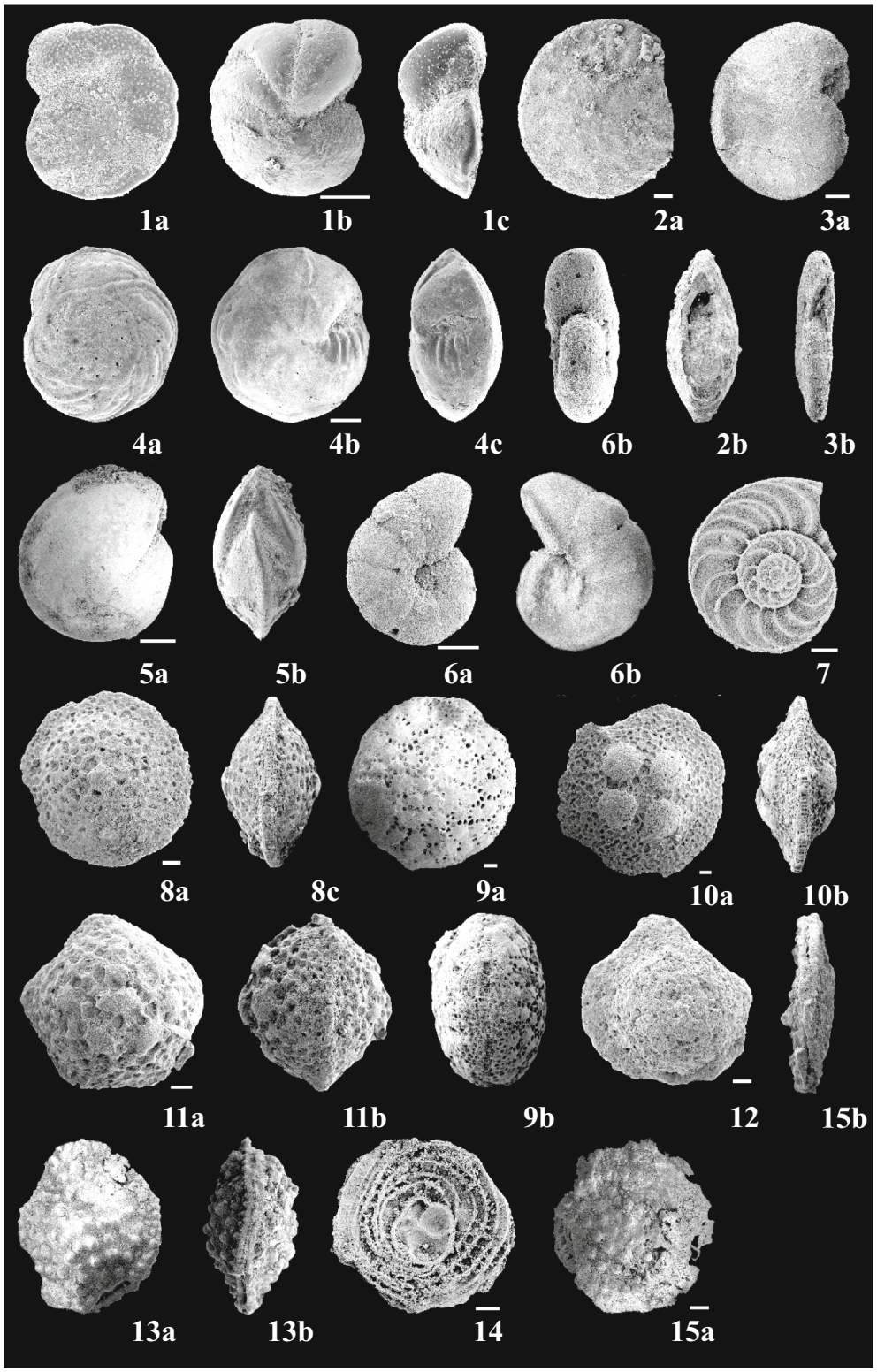


**Fig. 7. 1:** *Cibicides lobatulus* (Walker and Jacob) **2:** *Operculinella venosa* (Fichtel and Moll) **3,7:** *Operculina complanata* (Defrance) **4:** *Eponides repandus* (Fichtel and Moll) **5:** *Lenticulina suborbicularis* Parr **6:** *Anomalina collegerus* (Chapman and Parr) **8:** *Nephrolepidina verbeeki* Newlon and Holland **9:** *Nephrolepidina* sp. **10, 11:** *Nephrolepidina angulosa* (Provele) **12:** *Miogypsina* sp. **13:** *Cycloclypeus* (*Katacycloclypeus*) *carpenter* Brady **14:** *Cycloclypeus* (*Cycloclypeus*) *posteidae* Tan **15:** *Cycloclypeus* (*Katacycloclypeus*) sp. Scale 200 μm.

skeletons dissolved and preserved only as molds. Moreover, few coralline algae (0–20%, median 5%) and corals debris with a broad range (0–80%, median 5%), as well as scarce foraminifera (0–8%, median 2%) were recovered. Then, in the upper section (344–312 m), coralline algae (5–70%, median 20%) and foraminifera (0–10%, median 8%) increased more, with less common bryozoan fragments (0–20%, median 10%) and *Halimeda* (0–20%, median 7%), as well as sporadic coral fragments. As a whole, benthic foraminiferal abundance and species number, which ranged from 0 to 17speciesmen/slide (median 1) and 0–4 species/slide (median1) respectively, were much lower compared with the interval below. Planktic foraminifers were scarce. The stratum that yielded sufficient numbers of foraminifera to describe the assemblages were characterized by *Amphistegina* (*A. lobifera* and *A. lessonii*), with the median T/D value of *Amphistegina* ranging from 0.54 at 521–434 m to 0.51 at

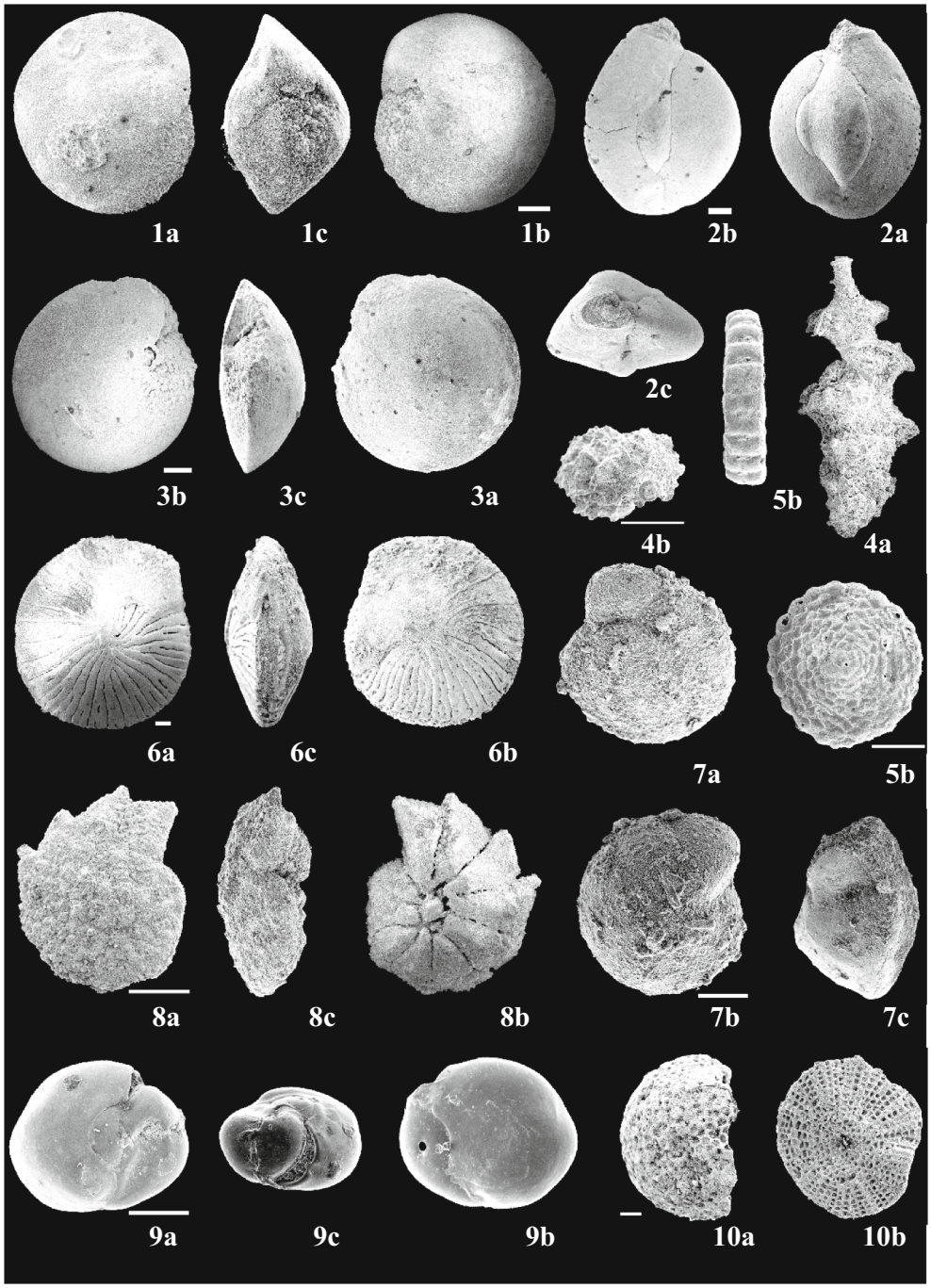


**Fig. 8. 1:** *Amphistegina lobifera* Larsen Scale **2:** *Quinqueloculina lamarckiana* d'Orbigny **3:** *Amphistegina lessonii* d'Orbigny **4:** *Shiphouvigerina porrecta* (Brady) **5:** *Sorites orbiculus* (Forskål) **6:** *Amphistegina radiata* (Fichtel and Moll) **7:** *Heterolepa praecinctus* (Karrar) **8:** *Calcarina praecalcar* n.sp. **9:** *Miliolinella labiosa* (d'Orbigny) **10:** *Gypsina globula* (Reuss) Scale 200 μm.

344–312 m, with the test size increasing upward.

*4.3.6. Amphistegina–Cycloclypeus–Operculina assemblage (FA6: 434–344 m, 8.49–5.30 Ma)*

This stratum starts with gray, fine to medium, moderately dolomitized coralline algal bindstone that alternated with dolomitized mudstone in the lower part of the section (434–378 m), overlain by yellow, strongly dolomitized coralline grainstoned and wackestone (378–344 m). In the lower section, coralline-algal (0–60%, median 20%) and coral fragments (0–50%, median 10%) dominated, with a few poorly preserved *A. lobifera* (0–5%, median 4%) and bryozoan fragments (0–10%, median 5%). Benthic foraminiferal abundance and species number ranged from 0 to 17speciesmen/slide (median 1) and 0–4 species/slide (median1) respectively. The 30 m-thick interval of upper section were mainly consisted of coralline algae (0–70%, median 30%), associated with scarce foraminifera (0–30%, median 4%). Coral were not encountered, except in the stratum between 372 m and 364.1 m. Foraminifera were totally benthic species, poorly preserved or dissolved, with 1–17 specimens/slide (median 2) and 1–6 species/slide (median 2). The foraminiferal assemblage was defined by the association of *Cycloclypeus*, *Miogypsina*, *Operculina* and common *A.lobifera.* The T/D values for *A.lobifera* ranged from 0.56 to 0.66, with median value of 0.56.

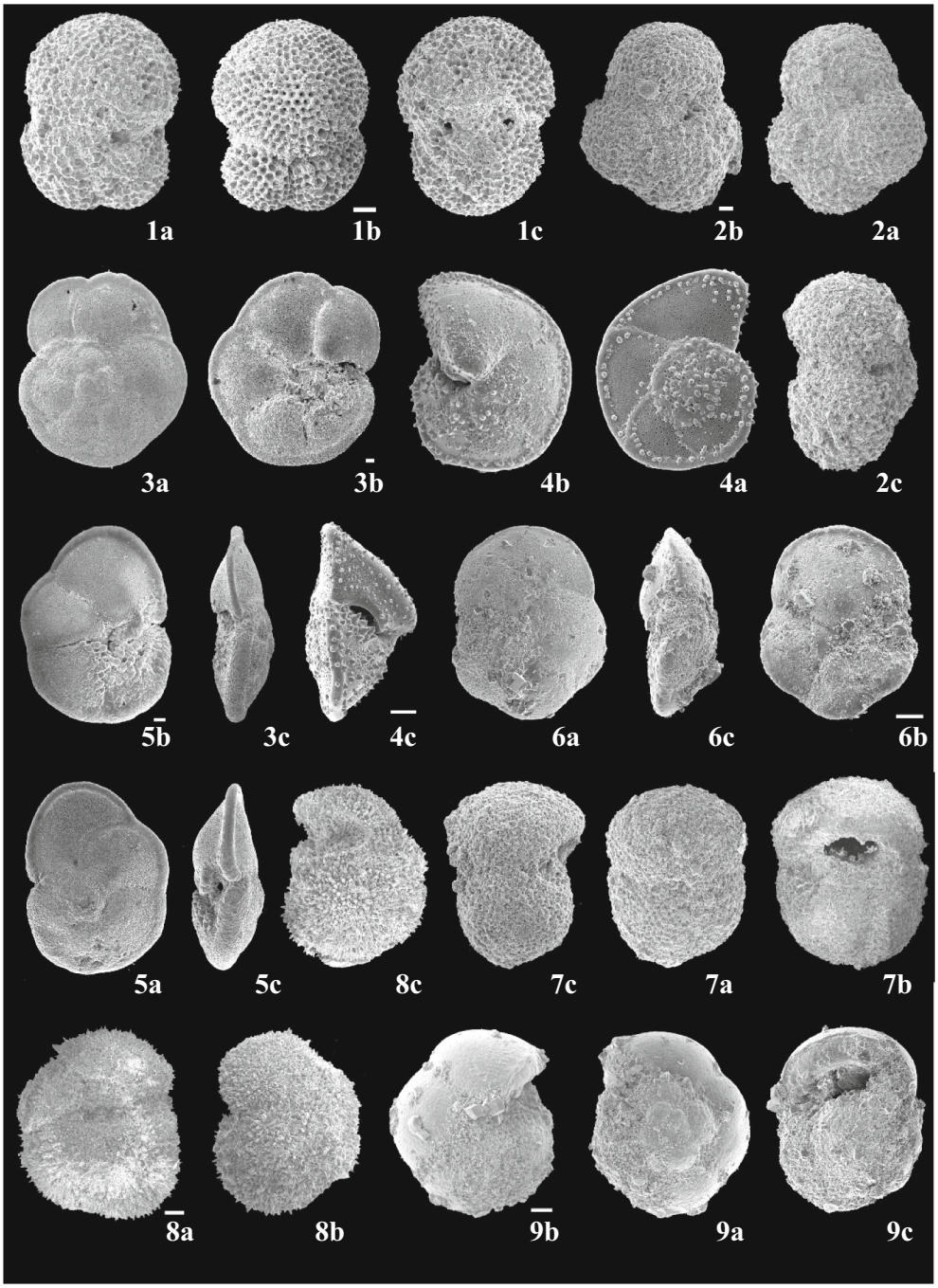


**Fig. 9. 1:** *Globigerinoides trilobus* (Reuss) **2:** *Sphaeroidinellopsis seminulina* (Schwager) **3:** *Globorotalia menardii* (d'Orbigny) **4:** *Globorotalia truncatulinoides* (d'Orbigny) **5:** *Globorotalia tumida* (Brady) **6:** *Globorotalia margaritae* (Bolli and Bermudez) **7:** *Globigerinoides obliquus* Bolli **8:** *Globoquadrina altispira* (Cushman and Jarvis) **9:** *Pulleniatina primalis* Banner and Blow Scale 50 μm.

*Mesophyllum, Lithothamnion, Lithophyllum* and rhodoliths were the most representative red algae.

#### *4.3.7. PF–Operculina–Cycloclypeus assemblage (FA7: 312–264 m, 4.35–3.16 Ma)*

The lithology changed from dark-gray, weakly dolomitized, coralline floatstone/wackestone and mudstone, upward to a white foraminiferal wackestone/grainstone/floatstone and mudstone. The predominant biological components were coralline algae (0–26%, median 8%) and foraminifera (10–50%, median 21%), as well as common bryozoan fragments (0–20%, median 10%), few *Halimeda* and bivalves. No coral was found. Foraminiferal tests were medium-good preserved. Benthic foraminifers were abundant (3–228 ind./gram, median 66), dominated by hyaline species with the median of 98%. Planktic species (0–123 ind./gram, median 8) took up about 30% of the total, mainly including *Globigerinoides trilobus*, *Globorotalia menardii*, *Globoquadrina globosa*, *Globigerinoides obliquus*, *Orbulina universa*, *Globigerinoides immaturus* and *Globigerinoides sacculifer*. The larger benthic foraminifers were mainly deeper-dwelling taxa, such as, *Cycloclypeus*, *Nummulities*, *Operculina*, *Amphistegina radiata* and *A. papillosa*. The T/D of *Amphistegina* in this section ranged from 0.29 to 0.61, with a median value of 0.41. The coralline algal fragments contain melobesioids (*Lithothamnium* and *Mesophyllum*) and abundant rhodoliths.

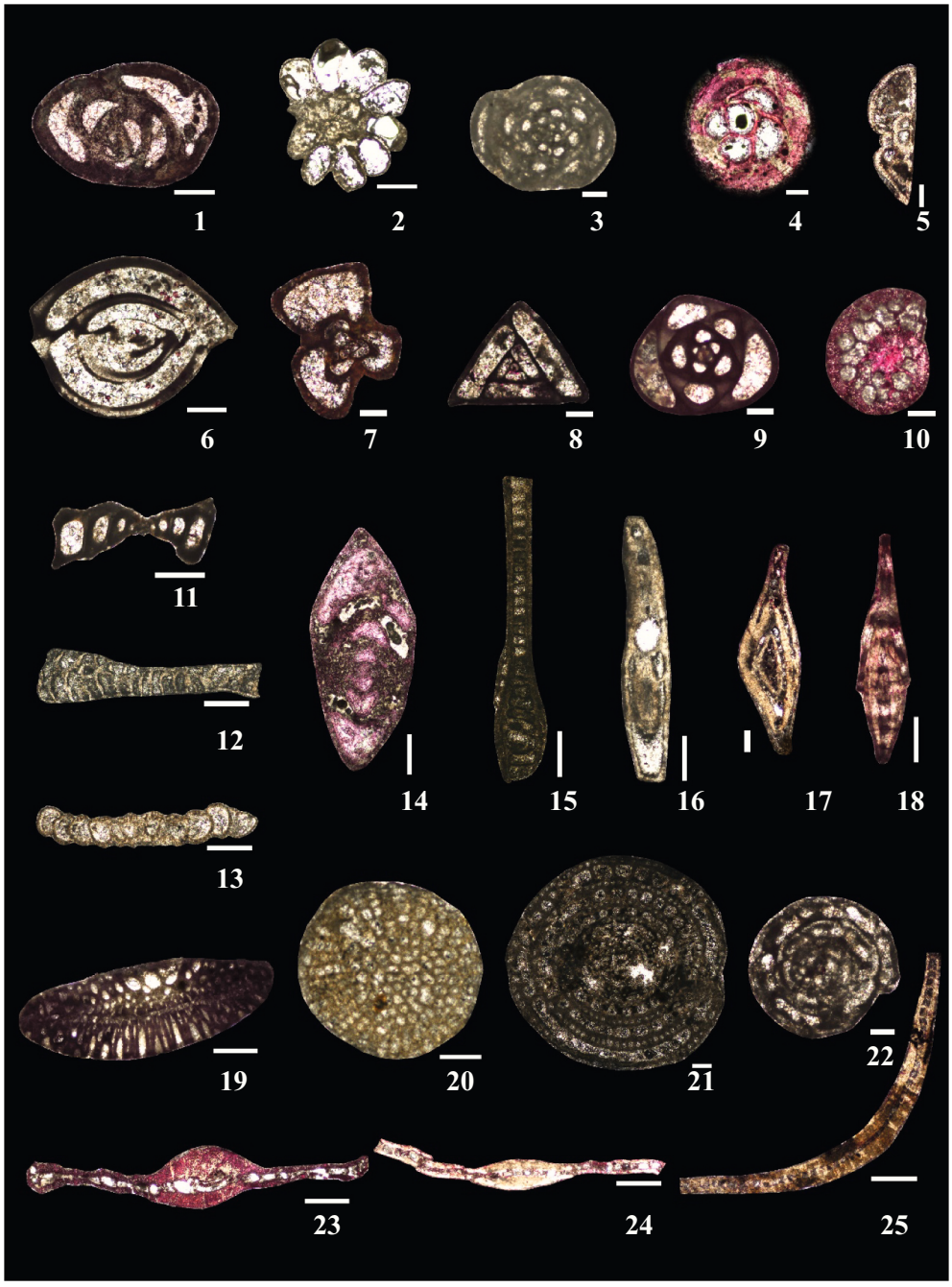


**Fig. 10. 1:** *Rosalina* sp.; scale 200 μm, 653.07 m **2:** *Calcarina calcar* d'Orbigny; scale 500 μm, 183.35 m **3:** *Cymbaloporetta* sp.; scale 100 μm, 554.07 m **4:** *Asterorotalia* sp.; scale 100 μm, 198.35 m **5:** *Cibicidina* sp.; scale 100 μm, 608.07 m **6:** *Pyrgo* sp.; scale 100 μm, 611.07 m **7:** *Triloculina* sp.; scale 100 μm, 608.07 m **8:** *Triloculina tricarinata* d'Orbigny; scale 100 μm, 611.07 m **9:** *Quinqueloculina* sp.; scale 100 μm, 557.07 m **10:** *Heterostegina suborbicularis* d'Orbigny; scale 100 μm, 243.50 m **11:** *Spiroloculina* sp.; scale 200 μm, 611.07 m **12:** *Marginopora vertebralis* Quoy et Gaimard; axialsection, scale 200 μm, 665.07 m **13:** *Planorbulinella larvata* (Parker & Jones); scale 200 μm, 563.07 m **14:** *Dendritina rangi* d'Orbigny; scale 200 μm, 653.07 m **15:** *Peneroplis* sp.; scale 200 μm, 637.92 m **16:** *Heterostegina suborbicularis* d'Orbigny; scale 200 μm, 291.50 m **17:** *Heterostegina curva* Moebius; scale 200 μm, 231.50 m **18:** *Operculinella* cf. *venosa* (Fichtel and Moll); scale 200 μm, 39.50 m **19:** *Cycloclypeus (Cycloclypeus) pillaria* BouDagher-Fadel; scale 500 μm, 363.00 m **20:** *Sphaerogypsina globula* (Reuss); scale 200 μm, 87.50 m **21:** *Flosculinella botangensis* (Rutten); scale 200 μm, 626.07 m **22:** *Alveolinella quoyi* (D'Orbigny); scale 100 μm, 611.07 m **23:** *Cycloclypenus indopacifics* Tan Sin Hok; scale 500 μm, 273.50 m **24:** *Cycloclypeus carpenteri* Brady; scale 200 μm, 288.50 m **25:** *Discocyclina ephippium* Schlotheim; scale 200 μm, 719.07 m.

*4.3.8. PF–Amphistegina assemblage (FA8: 258–198 m, 3.15–2.18 Ma)*

This lithology of this section is white, softly consolidated mudstone, coralline-foraminifera wackestone and packstone, overlained by coralline-foraminifera rudstone. The unsorted bioclastic components are mostly composed of coralline algae (0–60%, median 20%), foraminifera (0–40%, median 10%), bryozoan (0–85%, median 10%), with common echinoderm (0–10%, median 5%) and also few rhodoliths. Molluscan and coral fragments occur sporadically. The foraminiferal abundance and simple diversity were higher ranged from 0 to 49 ind./gram and 0–30 species/100 g, respectively, compared to the lower section. The foraminifers show poor-medium preservation, totally consisting of hyaline species. *Amphistegina* are represented by *A. lessonii*, *A. radiata* and subordinate *A. lobifera*. The planktic foraminifers (0–25%) were dominated by *Globigerinoides trilobus*, *Globorotalia menardii, Globoquadrina globosa*, *Globigerinoides obliquus* and *Orbulina universa*. Associated species are common *Numulities*, *Cycloclypeus*, *Calcarina* and few smaller benthic foraminifers such as *Heterolepa*, *Gypsina*, *Robulus* and Cibicides. The T/D of *Amphistegina* in this section ranged from 0.21 to 0.61, with a median value of 0.45.

*4.3.9. Amphistegina–Calcarina assemblage (FA9: 198–3 m, 2.18–0.089 Ma)*

The section is characterized by alternating layers of coralline-foraminiferal rudstone, coral framestone and coralline bindstone. The biota primarily consist wide range of coral (0–80%), coralline algae (0–60%) and foraminifera (0–30%). The foraminiferal abundance and diversity varied widely from 0 to 34 specimen/slide and 0–13 species/slide respectively. The foraminiferal tests were poorly preserved, mainly

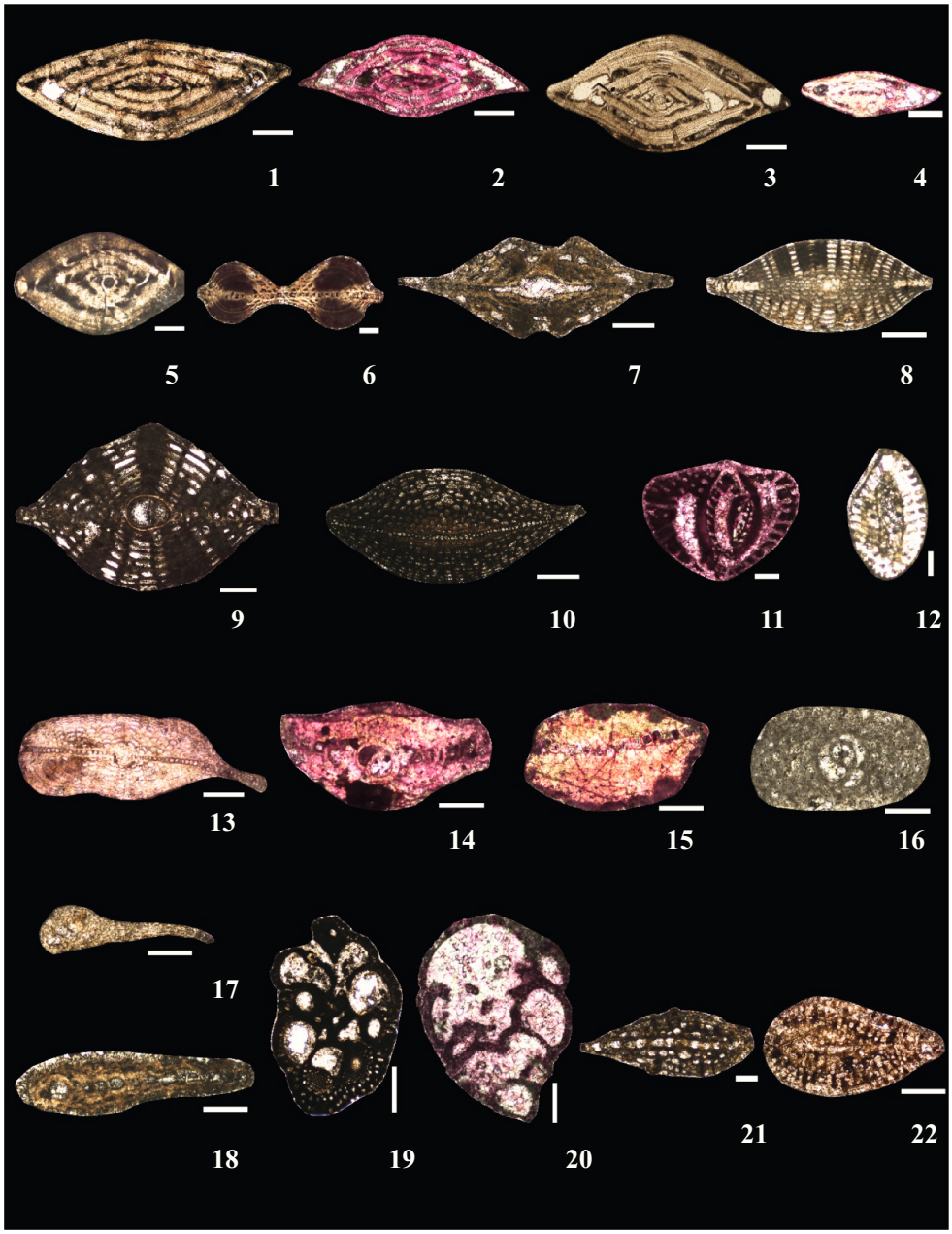


**Fig. 11. 1:** *Nummulites* sp.; scale 200 μm, 222.50 m **2:** *Amphistegina lessonii* d'Orbigny; scale 200 μm, 288.50 m **3:** *Amphistegina radiata* (FichtelandMoll); scale 200 μm, 195.50 m **4:** *Amphistegina papillosa*; scale 100 μm, 288.50 m **5:** *Amphistegina lobifera* Larsen Scale; scale 200 μm, 719.07 m **6:** *Nephrolepidina ferreroi* Provale; scale 200 μm, 637.92 m **7:** *Nephrolepidina angulosa* (Provale); scale 200 μm, 563.07 m 8: *Nephrolepidina sumatrensis* (Brady); scale 500 μm, 695.07 m **9:** *Nephrolepidina bikiniensis* Cole; scale 200 μm, 764.05 m **10:** *Nephrolepidina martini*; scale 500 μm, 630.34 m **11:** *Austrotrillina striata* Todd and Post; scale 100 μm, 551.07 m **12:** *Austrotrillina howchini* (Schlumberger); scale 100 μm, 789.85 m **13:** *Nephrolepidina ferreroi* Provale; scale 500 μm, 563.07 m **14:** *Miogypsinoides* sp.; scale 200 μm, 810.55 m **15:** *Miogypsinoides dehaarti* (van der Vlerk); scale 500 μm, 822.30 m **16:** *Eulepidina* sp.; scale 200 μm, 745.97 m **17:** *Miolepidocyclina banneri*; scale 500 μm, 578.07 m **18:** *Miogypsinoides formosensis* (Yabe and Hanzawa); scale 200 μm, 752.55 m **19:** *Victoriella* sp.; scale 500 μm, 764.05 m **20:** *Siphotextularia flintii* (Cushman); scale 200 μm, 653.07 m **21:** *Miogypsina borneensis* Tan; scale 200 μm, 585.74 m **22:** *MiogypsinoidesD dehaarti* (van der Vlerk); scale 500 μm, 855.55 m.

composed of hyaline species (median 80.9%). Planktic species took up the median of 6% of the total. Benthic foraminifers were characterized by *Amphistegina* (*A. lobifera* and *A. lessonii*) and, to a lesser extent, by *Calcarina*. The T/D of *Amphistegina* in this section range widely, from 0.42 to 0.73 with median level of 0.55. Coralline algae were dominated by *Lithophyllum*, *Jania* and *corallina*.

## 5. Discussion

### *5.1. Foraminiferal assemblages indicate the change of paleosedimentary facies and paleobathymetry*

The distinctness of foraminiferal species' ecological and microhabitat preferences make them invaluable for environmental reconstruction. The analysis of foraminiferal assemblages, dominating fossil components and carbonate texture resulted in eight different phases of deposition (units), which characterized the development of carbonate platform.

#### *5.1.1. Unit 1, reef front and reef flat facies (873.55–838 m, 19.6–18.67 Ma)*

The dominant miogypsinids–lepidocyclinids assemblages (FA1) in this unit indicate a shallow-water, euphotic environment with high energy (BouDagher-Fadel, 2008). The coarse-grained texture and poorly preserved foraminiferal tests with low abundance and species numbers, as well as the occurrence of *Amphistegina lobifera* further support the interpretation of shallow accumulation. The dominant coralline algae, *Jania* and *Amphiroa,* indicate intertidal or shallow subtidal environment with the water depth < 20 m (Kundal and Sanganwar, 1998). Strong wave action accelerated coral and coralline algal growth, resulting in the high deposit rate (about 193 m/Ma). Therefore, a coral-reef core and reef flat facies with water depths <15 m was proposed for this unit.

*5.1.2. Unit 2, open- platform facies interbedded with reef-flat facies (838–713 m, 18.67–17 Ma)*

These sections (838–762 m and 737.12–710 m) are dominated by FA2. Among FA2 taxa, *A. lobifera* tends to be prevalent in the upper euphotic zone with water depth within 10 m in modern reefs (Fujita et al., 2010). However, flat lepidocyclinids is typical of mesophotic environments at water depths of 30–70 m (Hallock and Glenn, 1985). Another meso-oligophotic genus, *Cycloclypeus,* was also found in this facies. In modern environments, *Cycloclypeus* only occurs the deepest oligophotic zone, at water depths ranging from 70 to 130 m (Hottinger, 1983; Hohenegger et al., 2000; Renema and Troelstra, 2001; Hohenegger, 2004; Renema, 2006, 2017). The melobesioid associations, such as *Lithothamnion* and *Mesophyllum*, are also indicative of water depth of >15 m in modern platforms (Adey, 1986), and can be found at depths of 110–120 m (Braga and Aguirre, 2004). The prevalence of lower-light (deeper-dwelling) foraminifera and coralline algae, combined with the mixture of shallow-water (e.g. *A. lobifera* and *Miogypsina*) and platform-interior species (e.g. *Austratrillina*, *Flosculinalla* and some miliolids) indicates a deeper platform setting into which shallower-dwelling taxa were likely transported by storm-waves and currents. Additionally, the lack of coral, and the increase of smaller benthic foraminifers and rhodoliths, as well as the higher foraminiferal species numbers, are indicative of increased mixing of facies, or possibly nutrient flux as indicated by relatively high Cu/Ti values (unpublished). Higher nutrient supply supports heterotroph suspension feeders instead of hermatypic corals, and reduces water transparency, which limits the depth range of photosynthetic autotrophs and symbiont-bearing organisms, including coralline algae and larger benthic foraminifera, and promotes the development of oligophotic assemblages at water depths of around 30 m or less. (Hallock, 1987; Hohenegger, 1995; Renema and Troelstra, 2001; Wilson and Vecsei, 2005; and others). The section of 762–737.12 m, dominated by FA1, with high depositional rates about 93 m/Ma, indicate shallower facies as produced in Unit 1.

*5.1.3. Unit 3, lagoon facies interbedded with lagoon slope facies (713–521 m, 17–10.19 Ma)*

The LBF rudstone and grainstone alternating with miliolids and small benthic foraminiferal wackestone and packstone, indicate the variation of water depth and hydroenergy. The occurrence of a larger number of imperforate miliolids (FA3), especially *Quinqueloculina* and *Triloculina* in fine-grained texture is generally taken as evidence for the slightly hypersaline shallow back-reef lagoon (Murray, 2006; Saidova, 2010; Parker and Gischler, 2015; Meng et al., 2020). This is consistent with the occurrence of *Halimeda*, which can thrive in relatively deep lagoon settings (Hallock, 2011), as has been well recorded in Nansha Islands (Yu et al., 1998), behind the Ribbon Reefs of the Australian Great Barrier Reef (Orme et al., 1978), and in Kapingamarangi Atoll (McKee et al., 1959). The sedimentation breaks, as exemplified by recurrent textural variations and the quantity variety of larger foraminifers (lepidocyclinids and *Amphistegina*), are indicative of periodic increase of current strength. Given the above, the index biology, the fine textures, the low sediment rate (<23 m/Ma), as well as the relative higher T/D value of *Amphistegina*, point to a tidal-current-influenced lagoonal and lagoon slope environment with palaeodepths on the order of 6–20 m.

*5.1.4. Unit 4, reef crest to reef front facies (521–378 m, 10.19–6.4 Ma)*

This upward deepening unit changes from reef-crest facies (521–434 m) to coralline-algal reef-core facies (434–378 m). At the lower section, dissolution of foraminifera generated moldic and vuggy porosity and the brown iron-oxide staining may indicate subaerial exposure at the low sea-level. Rare larger benthic foraminifera, common to rare corals debris with a broad range of coralline algae are interpreted as the reef-crest facies, with temporary exposures indicated by fenestral fabrics and seams. In the upper section, the dominant red algal bindstone and framestone has increased coral fragments, a few poorly preserved foraminifera (*A. lobifera*) (FA5) and increased bryozoan content indicated the mainly coral- coralline reef front facies in a slightly deeper water but still <20 m.

*5.1.5. Unit 5, reef front facies to reef-flat facies (378–312 m, 6.4–4.28 Ma)*

In this unit, an up-ward shallowing trend is suggested by the shift from shallow open-platform facies (378–344 m) to a reef flat facies (344–312 m). In the lower section, the foraminiferal assemblage (FA6) contains a mixture of deeper dwellers, such as *Cycloclypeus* and *Operculina*, and few shallow dwellers, such as *A. lobifera* and *Miogypsina*, indicating likely downslope transport. The presence of a few planktic foraminifers indicates open-marine influence, as do the prevalence of deeper-dwelling coralline algae such as *Mesophyllum* and *Lithothamnion*. The deeper reef front with water depth < 50 m was indicated by the biological components. In the upper section (344–312 m), the primrose-yellow packstone with scarce *Amphistegina* (FA5) that are partly dissolved, that is considered reef flat facies with the water depth < 10 m.

*5.1.6. Unit 6, deep open-platform facies (312–264 m, 4.28–3.16 Ma)*

The well preserved foraminifera and bryozoan fragments deposited in the poorly consolidated fine-grained matrix, combined with scarce coralline algae and lack of coral indicate non-reefal deposits that accumulated in calm, deep, normal-salinity marine environment (Flügel, 2010). The high value of P/B ratio, as well as the smaller rotaliines and deep-dwelling LBF (FA7) suggest deposition in the deeper part of the photic zone (Langer and Hottinger, 2000; Ćosović et al., 2004), considering the largest and flattest species of *Amphistegina* (*A. papillosa*) mostly occurred in the water depth of 95 m (Hohenegger, 2004). The specimens of *Amphistegina* in this facies have thickness-to-diameter ratios greater than those from any other facies. Overall, in this interval, the platform was at mesophotic depths in excess of 50 m, below the euphotic zone of prolific carbonate production, with the low deposit rate of 40 m/Ma, indicating a drowning phase (Schlager, 1981).

*5.1.7. Unit 7, deep open-platform to reef- front facies (264–198 m, 3.16–2.18 Ma)*

In this unit, the upcore textural variations from mudstone to rudstone indicate a shallow sequence. The dominance of planktic foraminifers (FA8) as well as the rich association of larger hyaline benthic foraminifers with low T/D values and rarity of porcellaneous taxa suggests a deep-platform setting. A mesophotic setting is indicated by the occurrence of larger, flat foraminifers such as *Cycloclypeus* and *Operculina* (Beavington-Penney and Racey, 2004; Pomar et al., 2017). The melobesioids associations consisting mainly of *Mesophyllum* and *Lithothamnion* again are characteristics of deeper photic environments (Adey, 1986), ranging from 15 m to nearly 120 m (Braga and Aguirre, 2004). The few shallow-dwelling corallines, such as, *Lithoporella*, may represent reworked material. The occurrence of rhodoliths in packstone are common in mesophotic settings, as was reported from 20 to 50 m water depth in southern Japan (Bassi et al., 2009), and 28–60 m in eastern Australia off Fraser Island (Lund et al., 2000). The depositional environment inferred from the analysis of lithology and foraminifera suggests the reef-front facies in mainly mesophotic environment at water depths around 20–40 m m.

*5.1.8. Unit 8, reef-flat and reef-front facie (198–3 m, 2.18–0.089 Ma)*

This interval likely represents a high to moderate energy environment indicated by poorly sorted, coarse sediment and abundant coral and coral algae. The corals taxa are reef-framework builders in this interval. In other strata, bird's-eye structures and stratified geopetal deposits are typical of a shallow tidal flat zone. *Amphistegina lobifera* and *Calcarina* spp. (FA9) frequently dominate recent foraminiferal assemblages in very shallow water of only a few meters depth (Hallock, 1999; Fujita et al., 2014), such as <10 m in Yongle atoll (Meng et al., 2020). The distribution of foraminiferal assemblages reflect hydrodynamics, for example, in the out reef flat, *A. lobifera* dominated, while on the more

sheltered inner reef flat and lagoon slope, *Calcarina hispital*, *Neorotalia*, miliolids and small rotallines become more prominent. The high T/D value of *Amphistegina* further supports it. The biotic association in this unit is typical of relatively shallow reef-flat to reef-front facies with water depths <20 m in modern tropical and subtropical marine carbonate environments.

### 5.2. The reconstructed paleobathymetry of Xisha area from foraminifera and sediment facies

Interpretation of paleobathmetric changes was based mostly on lithology, grain size, benthic foraminiferal index and palaeoecology, and diagnostic biological components. Our reconstructions indicate that paleobathymetry of CK2 fluctuated between 0 and nearly 100 m, and experienced two complete transgressive-regressive (T–R) depositional cycles, with the sequence boundary roughly corresponding to Late Miocene subaerial unconformity that lasted about 2 Ma (Fig. 6). The first T–R cycle (TB2, approximately 19.6–10.19 Ma) is characterized by FA1 at the basement, replaced in order by FA2 and FA3 interbedded with FA4 toward the top, indicating a relatively shallow-deeping-shallowing bathymetric sequence with a smaller water-depth oscillation. The changes of T/D of *Amphistegina* further support this interpretation (Fig. 6), which correspond to the change of global sea level (Haq et al., 1987). The sediment facies changed from the initiation of carbonate deposition, represented by platform facies progressing to a shallow lagoonal facies, indicating a gradual sea-level rise, then an irregular erosion surface occurred that represented an abrupt sea-level drop. The second T–R sediment cycle (TB3, about 10.19 Ma to recent) began with an erosional truncation, followed by the FA5/Unit 4 reef-crest facies during about 10.19–8.6 Ma, which is consistent with the phase of lowest sea-level in the SCS (Hao et al., 2000). The erosive regression was caused by the abrupt global sea-level drop of about 140 m at its maximum stage during the late Middle Miocene (Miller et al., 2020). The reef-crest facies was succeeded by reef front facies (FA5 and FA6/Unit 5), then deep platform facies (FA7/Unit 6) between 6.4 and 3.16 Ma. This succession represents a continuous increase of the relative sea-level to the deepest water setting during the early Pliocene to late Pliocene interval (4.3–3.16 Ma). The finest sediment textures and P/B ratios support the interpretation of a deep-platform setting. Subsequently, from the late Pliocene to the early Pleistocene, the appearance of FA8/Unit 7 indicates upperward shallowing. Since about 2 Ma, FA9/Unit 8 dominated the upper section of core, a further reduction in water depth.

The overall sedimentary sequence is characterized by a transgressive interval spanning from reef-crest and reef-bank facies to drowned platform facies, then a regressive interval spanning from the drowned-platform facies to shallow reef-bank and reef-core facies.

The paleobathymetric changes in the CK2 record (shallow-deep-shallow-deep-shallow) on the scales of millions of years since Early Miocene are in phase with the long-term trends of the third-order global cycles (Haq et al., 1987; Miller et al., 2020) and the Ying-qiong Basin sea-level oscillations in the SCS (Hao et al., 2000), revealing the significance of global sea-level change to the evolution of Xisha carbonate platform (Fig. 6). However, a notable difference from global sea-level curve is that the maximum flooding surface of second transgressive-regressive sequence (TB3) is much greater than that of the first one (TB2), which indicates that the superimposition of regional tectonic subsidence played an important role in the local sedimentary accretion.

### 5.3. The long-term evolution of Xisha carbonate platform validating the sea-level change

Carbonate accumulation is co-determined by accommodation space and carbonate supply, which are controlled by the interactions of eustatic changes, and tectonic, climatic, physic-chemical oceanic conditions, and the evolution of organisms (Pomar, 2001; Wilson, 2002). Three accumulation patterns record the sedimentary response to accommodation, such as aggradation and progradation, in contrast to loss of accommodation noted by retrogradation (James and Jones, 2016), which is consistent with three types of coral reefs development, i.e. catch-up, keep-up and give-up (Neumann and Macintyre, 1985). Based on the stratigraphy and foraminiferal assemblages recovered in the CK2 core, five stages of carbonate platform evolution can be recognized: initiation, slow development, shrinking and recovery, drowning, and recovery with rapid accretion (Fig. 12).

#### 5.3.1. Initial stage in the lower Early Miocene

Initiation of carbonate sedimentation occurred in the Early Miocene (19.6–17 Ma), characterized by reef core–shallow open platform–reef flat facies, with a high accumulation rates (~62 m/Ma). Due to the regional tectonic subsidence and global sea-level rise, the first frame-building coral and coralline algae start to aggradate on the platform

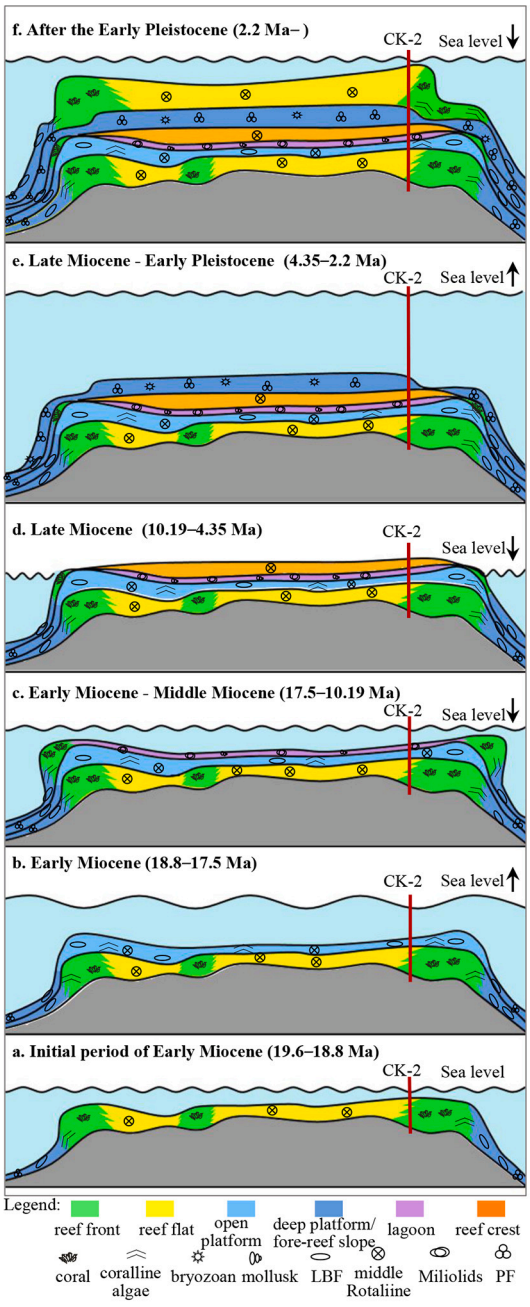


**Fig. 12.** Sketches showing the generalized developmental stages of platform reefs in Xisha region.

margin, producing compound reef buildups. They were partly eroded and transported to the interior by waves and currents, producing coralline rudstone and floatstone. The resulting relatively uniform shallow-water sequence indicated the deposition rate kept pace with accommodation space. Aggradation dominated, except for a short-term deepening at 17.5–18.8 Ma, represented by a more open-platform facies when possible increased nutrient flux reduced carbonate-accretion rates (e.g. Hallock and Schlager, 1986; Pomar, 2001; Halfar et al., 2004; Wilson and Vecsei, 2005). The strengthening of the Southeast Asian summer monsoon, which was recorded in many stations, such as, high mineralogical ratio chlorite / (chlorite + hematite + goethite) ($C_{RAT}$) value, low value of K/Al and high hematite/goethite, as well as black carbon index from ODP1148 station (Jia et al., 2003; Clift, 2020) and pollen index from north China (Jiang and Ding, 2008), resulted in upwelling currents that increase nutrient flux to the surface waters.

#### 5.3.2. Slow development stages from upper Early Miocene to Middle Miocene

Sedimentation in the upper Early Miocene–Middle Miocene (17–12.5 Ma) is characterized mainly by shallow lagoonal facies, except for the short-term reef flat facies at the 542–545 m and 560–563 m during the Mi3 (13.8 Ma) and Mi3a (14.8 Ma) Miocene Antarctic major ice-sheet expansion events, which resulted in about 50 m and 30 m global sea-level fall respectively (Miller et al., 2020). The accumulation rate declined by about a third (42.5 m/Ma), associated with lagoonal facies, which is typically lower than reef-flat and forereef facies (Kayanne, 1992). Although global sea-level gradually fell after 15 Ma, the relative sea-level remained about 6–10 m because of tectonic subsidence. Climate in Early to Middle Miocene was particularly favorable for coral-reef development, especially in the Mid - Miocene Climatic Optimum (MMCO), when coral reefs were most widely recorded (Wilson, 2008; Perrin and Bosellini, 2012; Wiedl et al., 2013). When accommodation creation cannot keep pace with reef growth, progradation and platform expansion can occur. The expansion of the Xisha carbonate platform in the middle Miocene is consistent with the thriving coral reefs in the SCS at this time (Wu et al., 2016).

#### 5.3.3. Shrink-restore stages in the Late Miocene

Platform development in the Late Miocene (12.5–4.35 Ma) occurred in two phase: a shrinking phase and a recovery phase (12.5–8.5 Ma), followed by resumption of platform accretion (8.5–4.35 Ma). A significant unconformity occurred at the uppermost Middle Miocene (12.55–10.19 Ma), with low accumulation rates (about 2.12 m/Ma) indicating an intermittent subaerial or submarine erosion. The timing of this interval corresponds to the Middle–Late Miocene Climate transition, that is, East Antarctic Ice Sheet grow to its peak by 12–10 Ma (Shackleton, 1975), resulting in the rapid, short-term global sea-level fall of about 78 m before 11.5 Ma (Haq et al., 1987). Next, reef-crest and reef-flat facies recovered on the unconformity, and then were replaced by fore-reef-core facies, indicating an upward deepening sequence, that resulted a catch up to give up interval. Accommodation space increased with global sea-level rise and tectonic subsidence; the reef responded with coralline algae as the pioneer carbonate producer. At the end of this interval (5.46–4.35 Ma), the shallow reef-flat facies indicates another catch-up phase.

#### 5.3.4. Drowning in the Pliocene to Early Pleistocene

The Pliocene to early Pleistocene (4.35–2.2 Ma) sequence is characterized by deep-platform facies to forereef-slope facies, with thin reef-flat facies interbedded. The lack of reef-constructing organisms in response to the global sea-level rise resulted in pelagic deposition, indicating a drowned platform facies (give-up phase). The change of foraminiferal assemblages indicates a deepening trend during the early–middle Pliocene global warming (4.35–3.26 Ma), then shallower facies corresponding with the increase of glacial activity and sea-level fluctuations with formation of the Arctic icecap at about 2.75 Ma in late Pliocene (Lisiecki and Raymo, 2005). Our results are consistent with the Wu and Zhang (2015) conclusion that the Xisha carbonate platform shrank during the Pliocene.

#### 5.3.5. Rapid development during the Early Pleistocene to Holocene

During the early Pleistocene to Holocene (2.2 Ma–), reef-flat facies alternated with reef-core facies with cycles of sea level. Transgression provided accommodation space for high carbonate accumulation rates, such as, from 1.3 to 1.7 Ma, with high proportions of coral and shallow-water foraminifers. The high carbonate deposition rate and increasing coral content indicate recovery (catch-up) and rapid aggradation (keep-up) of the coral reefs.

## 6. Conclusion

The CK2 core from Yongle Atoll yielded adequate planktic and larger benthic foraminifera to document biostratigraphy, except in the heavily dolomitized interval in the Middle to Late Miocene. Ranges of eleven age-diagnostic taxa were compared to published strontium-isotope data to construct the chronostratigraphy.

Among the total 141 foraminiferal taxa, nine foraminiferal assemblages were recognized representing eight well-determined carbonate facies with different paleobathymetry. miogypsinids–lepidocyclinids assemblage (873.55–840 m) indicated reef-flat facies with depth of <15 m. lepidocyclinids–*Amphistegina lobifera*–SBF assemblage (840–713 m) represented an open platform facies with water depth of <30 m. *M*iliolids–SBF (710–521 m) indicated lagoonal facies with water depth of ~10–30 m. *Amphistegina* assemblage (521–378 m, 348–312 m) represented reef-crest facies and/or coral-coralline algal reef facies with the depth approximately <20 m. *Cycloclypeus–Operculina–Miogypsina* assemblage (378–348 m) marked an coralline- reef front facies with the water depth < 50 m. PF–*Operculina–Cycloclypeus* assemblage (312–264 m) represented a drowning open platform facies with depth of 50–90 m. PF–*Amphistegina* assemblage (264–198 m) indicated transition from drowned platform facies to forereef-slope facies with the depth range from ~50 m. *Amphistegina–Calcarina* assemblage (198–3 m) represented the cycles of reef flat and shallow forereef-slope facies with the depth < 20 m. The sedimentological, foraminiferal and other paleontological data revealed two major sea-level cycles ("shallow-deep-shallow-deeper-shallow") since about 19.6 Ma coinciding with the global sea-level curve that influenced Xisha platform evolution in the Neogene.

We attribute the changes in facies and sedimentation rates to regional tectonism, sea-level fluctuations, and environmental factors, such as nutrient flux and climate change, that facilitated or limited carbonate production.

## Declaration of Competing Interest

The authors declare that they have no known competing financial interests or personal relationships that could have appeared to influence the work reported in this paper.

## Data availability

Data will be made available on request.

## Acknowledgements

We would thank Drs. Qi Shi, Hongqiang Yang, Huiling Zhang and Changqi Zhu for field work and helping in cutting the core. This work funded by the National Natural Science Foundation of China (Nos. 42030502 and 42090041). We sincerely acknowledge the editors and two anonymous reviewers for their constructive comments and suggestions, which greatly improved this manuscript.

## References


Abu-Zied, R.H., Bantan, R.A., 2013. Hypersaline benthic foraminifera from the Shuaiba Lagoon, eastern Red Sea, Saudi Arabia: their environmental controls and usefulness in sea-level reconstruction. Mar. Micropaleontol. 103, 51–67.

Adams, C.G., 1970. A reconsideration of the East Indian Letter classification of the Tertiary. British Museum (Natural history). Geology 19, 1–137.

Adams, C.G., 1984. Neogene larger foraminifera, evolutionary and geological events in the context of datum planes. In: Ikebe, N., Tsuchi, R. (Eds.), Pacific Neogene datum planes. University of Tokyo Press, Tokyo, pp. 47–67.

Adey, W.H., 1986. Coralline algae as indicators of sea-level. In: van de Plassche, O. (Ed.), Sea-Level Research. Springer, Dordrecht, pp. 229–280.

Anbuselvan, N., 2019. Benthic foraminiferal distribution and biofacies in the shelf part of Bay of Bengal, east coast of India. Mar. Biodivers. 49 (2), 691–706.

Baker, R.W., 1960. Taxonomic notes on the species figured by HB Brady in his report on the foraminifera dredged by HMS challenger during the years 1973–76. SEPM Spec. Publ. 9, 1–238.

Bassi, D., Nebelsick, J.H., Checconi, A., Hohenegger, J., Iryu, Y., 2009. Present-day and fossil rhodolith pavements compared: their potential for analysing shallow-water carbonate deposits. Sediment. Geol. 214 (1), 74–84.

Beavington-Penney, S.J., Racey, A., 2004. Ecology of extant nummulitids and other larger benthic foraminifera: applications in palaeoenvironmental analysis. Earth Sci. Rev. 67 (3–4), 219–265.

Berggren, W.A., Hilgen, F., Langereis, C., Kent, D.V., Obradovich, J., Raffi, I., Raymo, M. E., Shackleton, N., 1995. Late Neogene chronology: new perspectives in high-resolution stratigraphy. Geol. Soc. Am. Bull. 107 (11), 1272–1287.

Betzler, C., Chaproniere, G., 1993. In: McKenzie, J.A., Davies, P.J., Palmer-Julson, A., et al. (Eds.), Paleogene and Neogene Larger Foraminifera from the Queensland Plateau: Biostratigraphy and Environmental Significance, 133. Proc ODP, Sci. Results, pp. 51–66.

Blow, W.H., 1979. The Cenozoic Globigerinida: A Study of the Morphology, Taxonomy, Evolutionary Relationships and the Stratigraphical Distribution of Some of the Gobigerinida (Mainly Globigerinacea), 3. E.J. Brill Press, Leiden, pp. 1–1413.

Bolli, H.M., Saunders, J.B., 1985. Oligocene to Holocene low latitude planktic foraminifera. Cambridge University Press, pp. 155–262.

BouDagher-Fadel, M.K., 2008. The Cenozoic larger benthic foraminifera: the Neogene. Dev. Palaeontol. Stratigr. 21, 419–548.

Boudagher-Fadel, M.K., 2018. Evolution and Geological Significance of Larger Benthic Foraminifera, (Second Edition). UCL Press, p. 702.

Boudagher-Fadel, M.K., Banner, F.T., 1999. Revision of the stratigraphic significance of the Oligocene–Miocene 'Letter-Stages'. Revue De Micropaléontologie 42 (2), 93–97.

Boudagher-Fadel, M.K., Lokier, S.W., 2005. Significant Miocene larger foraminifera from South Central Java. Revue De Paleobiologie 24 (1), 291–309.

Boudagher-Fadel, M.K., Price, D.G., Koutsoukos, E.A.M., 2010. Foraminiferal biostratigraphy and paleoenvironments of the Oligocene–Miocene carbonate succession in Campos Basin, southeastern Brazil. Stratigraphy 7 (4), 283–299.

Braga, J.C., Aguirre, J., 2004. Coralline algae indicate Pleistocene evolution from deep, open platform to outer barrier reef environments in the northern Great Barrier Reef margin. Coral Reefs 23 (4), 547–558.

Cheng, T., Zheng, S., 1978. The recent foraminifera of the Xisha Islands, Guangdong Province, China I (in Chinese with an English abstract). Studia Mar. Sin. 12, 149–266.

Clift, P.D., 2020. Asian monsoon dynamics and sediment transport in SE Asia. J. Asian Earth Sci. 195 (104352), 1–11.

Ćosović, V., Drobne, K., Moro, A., 2004. Paleoenvironmental model for Eocene foraminiferal limestones of the Adriatic carbonate platform (Istrian Peninsula). Facies 50 (1), 61–75.

Dunham, R.J., 1962. Classification of carbonate rocks according to depositional texture. In: Ham, W.E. (Ed.), Classification of Carbonate Rocks–A Symposium, 1. AAPG Memoirs, pp. 108–121.

Embry, A., Klovan, E., 1971. A late Devonian reef tract on northeastern Banks Island, NWT. Bull. Can. Petrol. Geol. 19 (4), 730–781.

Fan, T., Yu, K., Zhao, J., Jiang, W., Xu, S., Zhang, Y., Wang, R., Wang, Y., Feng, Y., Bian, L., Qian, H., Liao, W., 2020. Strontium isotope stratigraphy and paleomagnetic age constraints on the evolution history of coral reef islands, northern South China Sea. Geol. Soc. Am. Bull. 131, 1–14.

Flügel, Erik, 2010. Microfacies of Carbonate Rocks Analysis, Interpretation and Application, 976. Springer, Berlin, p. 2004.

Folk, R.L., Word, W., 1957. Brasor rivers bars, a study in the significance of grain size parameters. J. Sediment. Res. 27 (1), 3–26.

Fujita, K., Omori, A., Yokoyama, Y., Sakai, S., Iryu, Y., 2010. Sea-level rise during termination II inferred from large benthic foraminifera: IODP Expedition 310, Tahiti Sea Level. Mar. Geol. 271 (1), 149–155.

Fujita, K., Nagamine, S., Ide, Y., Umezawa, Y., Hosono, T., Kayanne, H., Yamano, H., 2014. Distribution of large benthic foraminifera around a populated reef island: Fongafale Island, Funafuti Atoll, Tuvalu. Mar. Micropaleontol. 113, 1–9.

Geel, T., 2000. Recognition of stratigraphic sequences in carbonate platform and slope deposits: empirical models based on microfacies analysis of Palaeogene deposits in southeastern Spain. Palaeogeogr. Palaeoclimatol. Palaeoecol. 155 (3–4), 211–238.

Gradstein, F.M., Ogg, J.G., Hilgen, F.J., 2012. The Geologic Time Scale. Cambridge University Press.

Halfar, J., Godinez-Orta, L., Mutti, M., Valdez-Holguín, J.E., Borges, J.M., 2004. Nutrient and temperature controls on modern carbonate production: an example from the Gulf of California, Mexico. Geology 32 (3), 213–216.

Hallock, P., 1987. Fluctuations in the trophic resource continuum: a factor in global diversity cycles? Paleoceanography 2 (5), 457–471.

Hallock, P., 1999. Symbiont-bearing foraminifera. In: Modern Foraminifera. Springer, Dordrecht, pp. 123–139.

Hallock, P., 2011. Coral Reefs, carbonate sediments, nutrients, and global change. In: The History and Sedimentology of Ancient Reef Systems. Springer, Boston, MA, pp. 387–427.

Hallock, P., Glenn, E.C., 1985. Numerical analysis of foraminiferal assemblages: a tool for recognizing depositional facies in lower Miocene reef complexes. J. Paleontol. 59 (6), 1382–1394.

Hallock, P., Glenn, E.C., 1986. Larger foraminifera: a tool for paleoenvironmental analysis of Cenozoic carbonate depositional facies. Palaios 1, 55–64.

Hallock, P., Schlager, W., 1986. Nutrient excess and the demise of coral reefs and carbonate platforms. Palaios 1 (4), 389–398.

Han, C.R., Meng, X.Y., 1990. Foraminiferal fauna distribution in reef-facies beds since late Miocene in Xisha Islands and its significance (in Chinese with an English abstract). Mar. Geol. Quat. Geol. 10, 65–81.

Hao, Y.C., Chen, P.F., Wan, X., Dong, J., 2000. Late Tertiary sequence stratigraphy and sea level changes in Yinggehai Qiongdongnan Basin (in Chinese with English abstract). Geoscience 14, 237–245.

Haq, B.U., Hardenbol, J., Vail, P.R., 1987. Chronology of fluctuating sea levels since the triassic. Science 235 (4793), 1156–1167.

He, Y., Hu, P.Z., 1995. Early Miocene large foraminifera from biogenetic reef complexes of Dongsha Massif, South China Sea (in Chinese with an English abstract). Acta Palaeontol. Sin. 34 (1), 18–43.

Hohenegger, J., 1995. Depth estimation by proportions of living larger foraminifera. Mar. Micropaleontol. 26 (1), 31–47.

Hohenegger, J., 2004. Depth coenoclines and environmental considerations of western Pacific larger foraminifera. J. Foraminifer. Res. 34 (1), 9–33.

Hohenegger, J., 2005. Estimation of environmental paleogradient values based on presence/absence data: a case study using benthic foraminifera for paleodepth estimation. Palaeogeogr. Palaeoclimatol. Palaeoecol. 217 (1–2), 115–130.

Hohenegger, J., Yordanova, E., 2001. Displacement of larger foraminifera at the western slope of Motobu Peninsula (Okinawa, Japan). Palaios 16 (1), 53–72. https://doi.org/10.2307/3515552.

Hohenegger, J., Yordanova, E., Hatta, A., 2000. Remarks on West Pacific Nummulitidae (foraminifera). J. Foraminifer. Res. 30 (1), 3–28.

Hottinger, L., 1983. Processes determining the distribution of larger foraminifera in space and time. Utrecht Micropaleontol. Bull. 30, 239–253.

James, N.P., Jones, B., 2016. Origin of Carbonate Sedimentary Rocks. John Wiley and Sons, p. 446.

Jia, G., Peng, P., Zhao, Q., Jian, Z., 2003. Changes in terrestrial ecosystem since 30 Ma in East Asia: Stable isotope evidence from black carbon in the South China Sea. Geology 31 (12), 1093–1096.

Jiang, H., Ding, Z., 2008. A 20 Ma pollen record of East-Asian summer monsoon evolution from Guyuan, Ningxia, China. Palaeogeogr. Palaeoclimatol. Palaeoecol. 265 (1–2), 30–38.

Kayanne, H., 1992. Deposition of calcium carbonate into Holocene reefs and its relation to sea-level rise and atmospheric $CO_2$. In: Proc. 7th Int. Coral Reef Symp, 1, pp. 50–55.

Kundal, P., Sanganwar, B.N., 1998. Stratigraphical, palaeogeographical and palaeoenvironmental significance of fossil calcareous algae from Nimar Sandstone Formation, Bagh Group (Cenomanian–Turonian) of Pipaldehla, Jhabua Dt, MP. Curr. Sci. 75 (7), 702–708.

Langer, M.R., Hottinger, L., 2000. Biogeography of selected "larger" foraminifera. Micropaleontology 46, 105–126.

Li, B., Jian, Z., Li, Q., Tian, J., Wang, P., 2005. Paleoceanography of the South China Sea since the middle Miocene: evidence from planktonic foraminifera. Mar. Micropaleontol. 54 (1–2), 49–62.

Lisiecki, L.E., Raymo, M.E., 2005. A Pliocene–Pleistocene stack of 57 globally distributed benthic $\delta^{18}O$ records. Paleoceanography 20 (1), 1–16.

Loeblich, A.R., 1987. Foraminiferal Genera and their Classifications. Van Nostrand Rienhold Co, New York.

Lund, M., Davies, P.J., Braga, J.C., 2000. Coralline algal nodules off Fraser Island, eastern Australia. Facies 42 (1), 25–34.

Ma, Z., Li, Q., Liu, X., Luo, W., Zhang, D., Zhu, Y., 2017. Palaeoenvironmental significance of Miocene larger benthic foraminifera from the Xisha Islands, South China Sea. Palaeoworld 27 (1), 145–157.

Mateu-Vicens, G., Hallock, P., Brandano, M., 2009. Test shape variability of *Amphistegina* d'Orbigny 1826 as a paleobathymetric proxy: application to two Miocene examples. In: Demchuk, T., Gary, A. (Eds.), SEPM Spec. No. 93, Geologic Problems Solving with Microfossils, pp. 67–82.

McKee, E.D., Chronic, J., Leopold, E.B., 1959. Sedimentary belts in lagoon of Kapingamarangi Atoll. Am. Assoc. Pet. Geol. Bull. 43 (3), 501–562.

Meng, M., Yu, K.F., Hallock, P., Qin, G.Q., 2020. Distribution of recent foraminifera as depositional indicators in Yongle Atoll, Xisha Islands, South China Sea. Mar. Micropaleontol. 158, 1–15.

Meng, X.Y., 1989. Biostratigraphical boundaries and environmental changes of Xisha Islands since late Miocene shown by foraminiferal fauna. Acta Micropalaeontol. 6, 345–356.

Miller, K.G., Browning, J.V., Schmelz, W.J., Kopp, R.E., Wright, J.D., 2020. Cenozoic sea-level and cryospheric evolution from deep-sea geochemical and continental margin records. Sci. Adv. 6 (20), eaaz1346.

Murray, J.W., 2006. Ecology and Applications of Benthic Foraminifera. Cambridge University Press, New York, p. 426.

Murray, J.W., Lee, J.J., 1991. Ecology and distribution of benthic foraminifera. Biol. Foraminifera. 221–254.

Neumann, A.C., Macintyre, I.G., 1985. Reef response to sea-level rise: keep-up, catch-up, or give-up. In: Proceedings of the Fifth International Coral Reef Congress, Tahiti, 3, pp. 105–110.
Nigam, R., Heriques, P.J., 1992. Planktonic percentage of foraminiferal fauna in surface sediments of the Arabian Sea (Indian Ocean) and a regional model for paleodepth determination. Palaeogeogr. Palaeoclimatol. Palaeoecol. 91 (1–2), 89–98.
Orme, G.R., Flood, P.G., Sargent, G.E.G., 1978. Sedimentation trends in the lee of outer (ribbon) reefs, northern region of the Great Barrier Reef province. Philosophical transactions of the Royal Society of Lonndon. Ser. A Math. Phys. Sci. 291 (1378), 85–99.
Parker, J.H., Gischler, E., 2015. Modern and relict foraminiferal biofacies from a carbonate ramp, offshore Kuwait, northwest Persian Gulf. Facies 61 (3), 1–22.
Perrin, C., Bosellini, F.R., 2012. Paleobiogeography of scleractinian reef corals: changing patterns during the Oligocene –Miocene climatic transition in the Mediterranean. Earth Sci. Rev. 111 (1–2), 1–24.
Pomar, L., 2001. Ecological control of sedimentary accommodation: evolution from a carbonate ramp to rimmed shelf, Upper Miocene, Balearic Islands. Palaeogeogr. Palaeoclimatol. Palaeoecol. 175 (1–4), 249–272.
Pomar, L., Baceta, J.I., Hallock, P., Mateuvicens, G., Basso, D., 2017. Reef building and carbonate production modes in the west-central Tethys during the Cenozoic. Mar. Pet. Geol. 83, 261–304.
Qin, G.Q., 1981. The extinction of the Genus *Nephrolepidina* and preliminary investigation of the Pliocene/Miocene boundary in the northern South China Sea (in Chinese with an English abstract). Mar. Geol. Res. 1 (1), 93–100.
Qin, G.Q., 1987. A preliminary study on foraminiferal assemblages of well 1, Xiyong, Xisha Islands and their coral reef formation (in Chinese with an English abstract). Trop. Oceanol. Redai Haiyang. Guangzhou. 6 (3), 10–20.
Qin, G.Q., 1996. Application of micropaleontology to the sequence stratigraphic studies of late Cenozoic in the Zhujiang river mouth basin (in Chinese with an English abstract). Mar. Geol. Quat. Geol. 16 (4), 1–18.
Qin, G.Q., Zhu, X.H., 1982. Foraminifera assemblage of late Pleistocene of Shidao, Xisha Islands, and its geological significance (in Chinese with an English abstract). Mar. Geol. Res. 2 (4), 110–114.
Renema, W., 2005. Depth estimation using diameter-thickness ratios in larger benthic foraminifera. Lethaia 38 (2), 137–141.
Renema, W., 2006. Large benthic foraminifera from the deep photic zone of a mixed siliciclastic-carbonate shelf off East Kalimantan, Indonesia. Mar. Micropaleontol. 58 (2), 73–82.
Renema, W., 2007. Fauna Development of Larger Benthic Foraminifera in the Cenozoic of Southeast Asia. In: Biogeography, Time, and Place: Distributions, Barriers. and Islands. Springer, Dordrecht, pp. 179–215.
Renema, W., 2017. Terrestrial influence as a key driver of spatial variability in large benthic foraminiferal assemblage composition in the Central Indo-Pacific. Earth Sci. Rev. 177, 514–544.
Renema, W., Troelstra, S.R., 2001. Larger foraminifera distribution on a mesotrophic carbonate shelf in SW Sulawesi (Indonesia). Palaeogeogr. Palaeoclimatol. Palaeoecol. 75 (1–4), 125–146.
Saidova, K.M., 2010. Benthic foraminifer communities of the Persian Gulf. Oceanology 50 (1), 61–66.
Schlager, W., 1981. The paradox of drowned reefs and carbonate platforms. Geol. Soc. Am. Bull. 92 (4), 197–211.
Scholle, P.A., Ulmer-Scholle, D.S., 2003. A color guide to the petrography of carbonate rocks: grains, textures, porosity, diagenesis. AAPG Mem. 77 (77), 1–486.
Shackleton, N.J., 1975. Late cenozoic oxygen and carbon isotopic changes at DSDP Site 284: implications for glacial history of the northern hemisphere and Antarctica. Init Reps. Deep Sea Drill. Proj. 29, 801–807.
Wade, B.S., Pearson, P.N., Berggren, W.A., Pälike, H., 2011. Review and revision of Cenozoic tropical planktonic foraminiferal biostratigraphy and calibration to the geomagnetic polarity and astronomical time scale. Earth Sci. Rev. 104 (1–3), 111–142.
Wang, P.X., Zhao, Q.H., Jian, Z.M., Cheng, X.R., Huang, W., Tian, J., Wang, J.L., Li, Q.Y., Li, B.H., Su, X., 2003. Thirty million year deep-sea records in the South China Sea. Chin. Sci. Bull. 48 (23), 2524–2535.
Wang, Y.J., Gou, Y.X., Zhang, B.G., Xu, H., 1996. Studies of Miocene strata, biota and palaeoenvironment from Xi-Chen no.1 hole in Xisha Islands (in Chinese with an English abstract). Acta Micropalaeontol. 13, 215–223.
Wiedl, T., Harzhauser, M., Kroh, A., Coric, S., Piller, W.E., 2013. Ecospace variability along a carbonate platform at the northern boundary of the Miocene reef belt (Upper Langhian, Austria). Palaeogeogr. Palaeoclimatol. Palaeoecol. 370, 232–246.
Wilson, M.E.J., 2002. Cenozoic carbonates in Southeast Asia: implications for equatorial carbonate development. Sediment. Geol. 147 (3), 295–428.
Wilson, M.E.J., 2008. Global and regional influences on equatorial shallow-marine carbonates during the Cenozoic. Palaeogeogr. Palaeoclimatol. Palaeoecol. 265 (3), 262–274.
Wilson, M.E.J., Vecsei, A., 2005. The apparent paradox of abundant foramol facies in low latitudes: their environmental significance and effect on platform development. Earth Sci. Rev. 69 (1), 133–168.
Wu, S., Zhang, X., 2015. Response of Cenozoic carbonate platform on tectonic evolution in the conjugated margin of South China Sea (in Chinese with an English abstract). Earth Sci. J. China Univ. Geosci. 40 (02), 234–248.
Wu, S., Yang, Z., Wang, D., Lü, F., Lüdmann, T., Fulthorpe, C., Wang, B., 2014. Architecture, development and geological control of the Xisha carbonate platforms, northwestern South China Sea. Mar. Geol. 350, 71–83.
Wu, S., Zhang, X., Yang, Z., Wu, T., Gao, J., Wang, D., 2016. Spatial and temporal evolution of Cenozoic carbonate platforms on the continental margins of the South China Sea: response to opening of the ocean basin. Interpretation 4 (3), 1–19.
Yu, K.F., Zhao, H.T., Zhu, Y.Z., 1998. Modern sedimentary characteristic of Halimeda on coral reefs of Nansha Islands (in Chinese with an English abstract). Acta Sedimentol. Sin. 16 (3), 20–24.
Zachos, J., Pagani, M., Sloan, L., Thomas, E., Billups, K., 2001. Trends, rhythms, and aberrations in global climate 65 Ma to present. Science 292 (5517), 686–693.
Zheng, S.Y., 1979. The recent Foraminifera of the Xisha Islands, Guangdong Province, China, Part 2 (in Chinese with an English abstract). Studia Mar 15, 101–232.